

# Supplementary information

## Table of Contents

<b>Supplementary discussion:</b> .....	<b>3</b>
<b>How do SNARE ligands enhance opening of the fusion pore?</b> .....	<b>3</b>
Membrane curvature as a driving force .....	3
The energy stored in the imposed membrane curvature .....	5
The peristaltic force on HOPS .....	6
Influence of HOPS on the pulling force of SNARE transmembrane domains .....	6
HOPS-induced membrane tension .....	7
Effect on the free energy barrier of the fusion pore .....	8
Acceleration of fusion pore formation .....	9
<b>Materials and Methods</b> .....	<b>11</b>
<b>Strains and culture conditions</b> .....	<b>11</b>
Table S1: Yeast strains used in this study .....	11
Table S2: Primers used for genetic manipulations .....	12
<b>Vacuole isolation</b> .....	<b>13</b>
<b>Vacuole fusion and content mixing assay</b> .....	<b>13</b>
<b>Lipid mixing assay</b> .....	<b>14</b>
<b>Immunoprecipitations</b> .....	<b>14</b>
<b>Gel electrophoresis and Western blot</b> .....	<b>14</b>
<b>FM4-64 staining</b> .....	<b>15</b>
<b>Affinity purification of antibodies</b> .....	<b>15</b>
<b>Papain digestion and F<sub>ab</sub> fragment purification</b> .....	<b>16</b>
<b>Purification of rVam7</b> .....	<b>16</b>
<b>Purification of HOPS, HOPS subcomplexes and CORVET</b> .....	<b>17</b>
<b>Rapamycin-induced protein re-localisation</b> .....	<b>17</b>
<b>Statistics for biological experiments</b> .....	<b>17</b>
<b>Simulation model and settings</b> .....	<b>18</b>
<b>Modeling the vacuolar SNARE complex</b> .....	<b>18</b>
<b>Membrane simulation setups</b> .....	<b>19</b>
Table S3: Overview of the different simulation systems. ....	19
<b>Model and setup of the HOPS simulations</b> .....	<b>20</b>
<b>Free energy of fusion and SNARE forces</b> .....	<b>21</b>
Table S4: Overview of the two different umbrella sampling protocols. ....	21
<b>Bending energy and force</b> .....	<b>22</b>
<b>Continuum model</b> .....	<b>23</b>
<b>Code availability</b> .....	<b>24</b>
<b>Supplementary References:</b> .....	<b>25</b>
<b>Supplementary Figures:</b> .....	<b>28</b>
<b>Figure S1: Reagents.</b> .....	<b>28</b>
<b>Figure S2: Kinetics and efficiency of in vitro vacuole fusion, measured by content mixing.</b> .....	<b>30</b>
<b>Figure S3: HOPS and CORVET complexes stimulate fusion to similar degrees.</b> .....	<b>31</b>
<b>Figure S4: ypt7<math>\Delta</math> vacuoles require both Vam7 and HOPS for content mixing.</b> .....	<b>32</b>
<b>Figure S5: A molecular crowding agent cannot stimulate fusion in the absence of bulky SNARE ligands.</b> .....	<b>33</b>
<b>Figure S6: Effect of rapamycin-induced dimerization on in-vivo vacuole fusion using the small fusion protein FRB-GFP.</b> .....	<b>34</b>

<b>Figure S7: Fusion can be prematurely triggered by protein recruitment after osmotically induced vacuole fragmentation. ....</b>	<b>35</b>
<b>Figure S8: Effect of HOPS on the free energy barrier of fusion pore formation. ....</b>	<b>36</b>
<b>.....</b>	<b>38</b>
<b>Figure S9: Detailed analysis of HOPS-mediated membrane bending in the presence of an inter-membrane restraint. ....</b>	<b>38</b>
<b>Figure S10: Effect of HOPS on the force exerted by a single SNARE complex. ....</b>	<b>40</b>

## Supplementary discussion:

### How do SNARE ligands enhance opening of the fusion pore?

#### ***Membrane curvature as a driving force***

HOPS appears to contribute two separable functions to vacuole fusion. It catalyzes SNARE complex assembly<sup>1-4</sup>, which is necessary for membrane docking and the induction of hemifusion. However, it also binds to the assembled SNARE complex<sup>5</sup> and, as we show here, this interaction promotes the formation or expansion of the fusion pore. This second function can explain why Vps33 with amino acid substitutions can support normal trans-SNARE pairing and lipid mixing but not content mixing<sup>6</sup>. It is also compatible with subsequent studies on liposome fusion, which found that the addition of the Vps33-containing HOPS complex not only increased SNARE complex formation several-fold, but also led to a disproportionately higher increase in content mixing<sup>7</sup>. While there is a priori no reason to assume that SNARE complex density should be linearly related to the rate of content mixing, this result is consistent with the steric effects of HOPS on the fusion site that we describe here.

Another unexplained finding is that SNARE ligands such as Sec17/ $\alpha$ -SNAP and Sec18/NSF, which are normally involved in SNARE complex disassembly, can stimulate liposome fusion under certain conditions<sup>8</sup>. They are particularly effective when used in conjunction with a non-hydrolysable ATP-analog, which stabilizes SNARE/ $\alpha$ -SNAP/NSF complexes<sup>9</sup>. Also the fusion of intact vacuoles can be stimulated by Sec17/ $\alpha$ -SNAP, but only if complete SNARE complex zippering is prevented by a C-terminal truncation of the Q<sub>c</sub>-SNARE Vam7<sup>10</sup>. On vacuoles with wildtype SNAREs, release of Sec17 from the membrane is necessary for fusion<sup>11</sup> and addition of Sec17 is even inhibitory<sup>12</sup>. It has been argued that binding of Sec17 might stimulate fusion by stabilizing or ordering incompletely zippered SNAREs<sup>10</sup>. This raises the question whether binding of HOPS or of SNARE antibodies might promote fusion by favoring the transition from partially zippered to fully zippered SNARE complexes. We consider this as unlikely for several reasons. First, full zippering of SNAREs is necessary to efficiently reach lipid mixing<sup>10</sup>. Since vacuoles reach a hemifused state in our experiments, we can expect them to have zippered SNARE complexes. Second, HOPS binds SNARE complexes through Vps33 and in our experiments Vps33 alone acts as a competitive inhibitor of fusion (Figs. 1,2). But

when the effective size of Vps33 is increased by addition of monoclonal antibodies to a C-terminal peptide tag of this protein, fusion is strongly stimulated. Since this monoclonal antibody does not recognize the SNAREs, it is difficult to conceive how it might have a structuring or ordering effect on partially zippered SNARE complexes. Third, in vivo vacuole fusion can be triggered by recruiting the bulky phosphofruktokinase to the SNARE complex, which is completely unrelated to fusion and unlikely to undergo any direct interaction with SNAREs. Thus, stimulation by a simple increase in SNARE complex volume remains the most suitable interpretation. By analogy, we propose that also Sec17/ $\alpha$ -SNAP and Sec18/NSF, of which several units can bind the SNARE complex at a time <sup>13</sup>, stimulate liposome fusion by acting as bulky ligands that deform the fusion site. This model is also consistent with the observation that the membrane-intercalating sequences of Sec17/ $\alpha$ -SNAP are dispensable for fusion as long as full-length, wildtype SNAREs are used <sup>9</sup>.

Since we can stimulate the transition from hemifusion to full fusion by bulky SNARE ligands, the SNARE domains must be sterically accessible in these intermediates. We posit that the hemifusion zone behaves like a Brownian ratchet. Spontaneous shape fluctuations of the apposed membranes might liberate the space for bulky SNARE ligands, which, once bound, fix the system in this spontaneously created, highly curved or "tense" state. Thereby, they will increase the probability of pore opening or expansion relative to the "relaxed" state, in which fluctuations into the highly curved state would be short-lived and the probability for pore formation would remain low.

Electron microscopy structures of HOPS feature a SNARE-binding domain (head region) of approximately 12-14 nm diameter, which probably encapsulates the SNARE complex <sup>14,15</sup>. Binding this head region to SNAREs will markedly affect the geometry of the hemifusion stalk, which restrains the apposed membranes from separating and thereby enforces strong local membrane curvature. On first sight, it may seem trivial to relate the HOPS-induced high curvature to enhanced fusion activity. Inducing curvature-stress is a well-accepted mechanism to accelerate fusion <sup>16</sup> and small vesicles are more 'fusogenic' than large ones <sup>17</sup>. However, fusion does not relax the curvature-stress that HOPS imposes on the two flat membranes in an immediately apparent way (Fig. 4a & Fig. S8) and other factors, such as peristaltic forces and increased pulling on the SNARE transmembrane domains might play

major roles. The driving force that HOPS contributes to fusion pore opening is thus not obvious – necessitating theory and simulations in order to explore its sources.

### ***The energy stored in the imposed membrane curvature***

To gain insights into the bending energy (stress) imposed on the fusion site by the HOPS-SNARE complex, we performed both molecular dynamics (MD) simulations and elastic continuum modeling (see *Methods*). Although a recent study reported the existence of extended hemifusion diaphragms between yeast vacuoles fusing in vitro<sup>18</sup>, our own studies by light and electron microscopy did not reveal extended hemifusion zones at a sufficient frequency to permit their quantification and interpretation (D'Agostino and Mayer, in preparation). Therefore, our models assume a stalk as the hemifused structure. Our conclusions would not qualitatively change if the hemifused structure were a diaphragm. In the MD simulations, we derived the work that HOPS must perform to bend the membrane and counteract the (partial) pressure that the membrane exerts on the surface of HOPS. In mechanical equilibrium, the bending work, which HOPS must perform to conserve the membrane shape of minimal free energy, equals the exerted pressure ( $P$ ) times the volume ( $V$ ) of HOPS. For a purely repulsive sphere this will approximate the bending energy of the adopted shape. The elastic continuum model underestimates the actual bending work by about a factor of two (see *Methods* for a detailed explanation). This bending energy (equilibrium bending work) amounts to about 150  $k_B T$  (12 nm HOPS sphere) to 230  $k_B T$  (14 nm HOPS sphere) (Fig. S9b). These values are, however, subject to the approximation of shape, the location with respect to the stalk (e.g. Fig. S9c), and the location within the vacuole-vacuole contact zone (at the curved periphery of the contact zone, called the vertex ring<sup>19</sup>, these values will likely be lower). Since HOPS catalyzes SNARE complex assembly, we expect that a substantial fraction of the bending work will be overcome by SNARE complex formation ( $\sim 65 k_B T$  per SNARE complex<sup>20</sup>). Furthermore, HOPS tethers membranes through Rab-GTPases and direct lipid interaction<sup>21,22</sup>. To discern whether the acceleration of fusion might rely on the absence or presence of tether activity, we additionally modeled a HOPS with tether activity (coined '14 nm HOPS attractive') by including weak attractions between the surface of HOPS and the membrane. These surface attractions can render the average performed bending work negative (Figure S9b; green line). This implies that the bending energy is fully compensated by the favorable surface attraction and that the presence of HOPS will spontaneously curve the membrane

also in the absence of the stalk. However, these attractions do not imply that the bending energy and thus the stress imposed on the adherent membranes vanishes (see  $F_{\text{bending}}$  in Fig. S9b,d).

### ***The peristaltic force on HOPS***

To gain insight into the force required to restrain HOPS at the fusion site, we estimated the peristaltic force  $f_d$ , which pushes HOPS away from a stalk, a fusion pore, or a SNARE complex. It originates from the induced membrane curvature and may be enhanced by osmotic pressure of the fusing vesicles. Both our MD simulations and the elastic continuum model estimate the curvature-induced component of this force to be several 10s of pN, up to 60 pN, when HOPS binds close to the fusion site (Fig. S9b,d). Intuitively, we expect  $f_d$  to decrease when HOPS is located at the vertex, i.e. at the already curved periphery of the vacuole-vacuole contact zone. However, while surface attractions (membrane tethering) reduce  $f_d$  by half in the MD simulations (Fig. S9b), they do not give rise to a free energy minimum near the constraint, as shown by our continuum model (Fig. S9d). Therefore, HOPS can only be kept near the constraint by binding to the SNARE complex, which counteracts  $f_d$ .

### ***Influence of HOPS on the pulling force of SNARE transmembrane domains***

Vice versa, HOPS will exert a pulling force on the SNARE C-termini, which are thought to approach each other during the progression from hemifusion to pore opening until they closely associate as observed in the neuronal SNARE complex<sup>23</sup>. To estimate to which degree bulky SNARE complex ligands, such as HOPS, may alter the force that SNARE TMDs exert on the luminal leaflets (Fig. S10a), we performed coarse-grained molecular dynamics simulations. We rationalized the gain in force from the reduction in relative work ( $\Delta\Delta G$ ) (Fig. S10b) required to *slightly* bring the luminal C-termini of Vam3 and Nyv1 into closer proximity. The corresponding forces on the SNARE TMDs were derived from this relative work (Fig. S10c). With *slightly* we emphasize that the here-imposed stalk indentation is reversible, meaning that the stalk will recover upon removal of the external force (no fusion barrier is being crossed).

HOPS reduces the relative work that the SNARE complex must perform to (slightly) indent the stalk by up to 12  $k_B T$  (Fig. S10b). The corresponding apparent 'force gain'

is given by the derivatives of this work function (Fig. S10c). Its magnitude of 10-30 pN suggests that HOPS binding would gain the equivalent of one SNARE complex<sup>20,24,25</sup>. Its magnitude shows a high offset value which gradually converges as the C-termini approach each other. In contrast, simulations where the juxta-membrane regions between the coiled-coil and transmembrane domains were modeled as fully flexible (unstructured) - rendering the SNARE complex mechanically ineffective for transmitting bending force to its TMDs - showed a lower but constant 'force gain' (8 pN for 14 nm "HOPS", Fig S10c). This illustrates that the initial apparent force gain largely depends on the mechanical stiffness of the SNARE linkers. It likely originates from a projection of the peristaltic force on the SNARE C-termini. This is not necessarily intuitive since the stalk imposes an inter-membrane constraint and therefore one might expect that the imposed stress tends to stretch the stalk rather than ease its indentation.

The observed force gain is compromised by positioning "HOPS" more distally with respect to the stalk (Fig. S10b,c; HOPS 12 nm (linker)). This suggests that the force gain is mediated by direct steric effects of HOPS on the site of hemifusion. Although the force gain is substantial with respect to the inherent force exerted by a SNARE complex – doubling or even tripling the effective SNARE force -- the concomitant gain in free energy, i.e., the driving force of fusion, remains (I) relatively small ( $\sim 10 k_B T$ ) and (II) largely relies on the mechanical stiffness and thus the adopted secondary structure of the HOPS-bound SNAREs.

### ***HOPS-induced membrane tension***

The curvature induced by HOPS reduces the effective, projected area of the proximal leaflets via corrugation of the membrane surface. This may result in a concomitant surface tension. It is unclear whether such a (local) tension could relax (dissipate) via lipid diffusion, solvent efflux and/or lipid flip-flops (in case of asymmetric leaflet tension or spontaneous curvature). We used our continuum model to estimate the membrane area ( $A-A_0$ ) that would be required to compensate for this tension induced by the presence of HOPS (Fig. S9c). A single HOPS sphere, which is closely restrained to the fusion site, will reduce the area of the membrane-membrane contact zone by  $\sim 70 \text{ nm}^2$ . Although this may in principle generate significant tension at high densities of HOPS on the membrane, we can effectively rule out tension as a main cause of accelerated fusion due to our experimental

observations: Displacing bulky SNARE ligands from the SNARE complex via a flexible linker of 35 amino acids abolishes the stimulation of fusion by them (Fig. 3). But the required excess membrane area ( $A-A_0$ ), and thereby the tension that HOPS might induce, depends only weakly on the distance of HOPS ( $d$ ) from the inter-membrane constraint – quite in contrast to  $F_{\text{bending}}$  and  $f_d$  (Figure S9c,d). Therefore, tension should not provide the main driving force for the observed acceleration of fusion.

### ***Effect on the free energy barrier of the fusion pore***

We explored the effect of 'HOPS' on the free energy barrier of fusion pore formation using a previously published method<sup>26</sup>. In order to estimate the free energy required to open the fusion pore, we pull two hydrophilic 'beads' (probes; colored purple in Fig. S8b-d) towards each other near the center of the stalk. Each probe is comprised of 8 clustered solvent beads. Bringing the probes in closer proximity exerts a squeezing force on the stalk which enforces its expansion (evolution). The “stalk thickness” is defined by the distance between the two probes. The idea of this approach is that one brings the system close to a nucleation barrier until the barrier can be crossed spontaneously within the simulation time scales. The work required to enforce nucleation gives an estimate of the height of the barrier. An advantage of this approach is that we can use the same reaction coordinate to test whether there is a propensity for 'leaky' fusion (coined leakage pore mediated stalk elongation<sup>26</sup>). For more detailed information see our previous work<sup>26</sup>.

The membrane system that we simulated consists of a POPC:POPC mixture (40% POPE) with a fusion site comprised of one HOPS-bound SNARE complex and two additional unbound SNARE complexes (see Fig. S8a and *Methods*). Tension-less membrane conditions are ensured by the presence of free membrane edges which allow fast spontaneous lipid flip-flops between the leaflets and free adaptation of membrane area. The presence of the HOPS sphere substantially reduces the free energy barrier of fusion pore formation, from 67  $k_B T$  to 34  $k_B T$  (Fig. S8a). A striking barrier of 67  $k_B T$  – despite the presence of three SNARE complexes – illustrates how ‘trapped’ the fusion reaction is after stalk formation. Furthermore, metastable hemifusion diaphragms, i.e., hemifusion states of the thickness of a single membrane, have not been observed in the simulations, suggesting that the stalk to fusion pore transition faces only a single free energy barrier. Since HOPS is

assumed to tether membranes in vivo<sup>21,22,27</sup>, it is important to test whether the observed ‘fusion acceleration’ is conserved (if not enhanced) even in the presence of membrane tethering, which we have approximated by making HOPS membrane-attractive (no net bending work; Fig. S9b). This is the case. The pronounced reduction of work required to open the fusion pore can thus be attributed to a substantial shift in the nucleation barrier towards larger probe to probe distances (the arrows in Fig. S8a). In other words, opening of the fusion pore requires way less squeezing of the stalk – and thus less work – in the presence HOPS. This results in a more than 30  $k_B T$  decrease of the fusion barrier and thereby a dramatic acceleration ( $>e^{30}$ ) of the subsequent fusion reaction.

### ***Acceleration of fusion pore formation***

Based on the preceding considerations, we propose two possible sources for the observed acceleration of fusion pore formation by HOPS:

(I) Relaxation of curvature stress. The progression of SNARE zippering into the juxta-membrane and transmembrane domains upon fusion pore opening moves HOPS further away from the fusion site – it increases the distance  $d$  in Fig. S9 by about 1 nm (see the table in Fig. S9b). HOPS thereby imposes less of a steric constraint. The continuum model illustrates that the bending energy ( $F_{\text{bending}}$ ) features a sharp, initial reduction when a nearby located HOPS complex moves slightly away from the stalk. From the MD simulations, we estimate that fusion pore formation reduces the bending work that HOPS performs by about 50  $k_B T$ . This partial, relative release of bending stress may very well drive subsequent fusion pore opening.

(II) Geometrical compatibility. Fusion pore formation involves the formation of pronounced ‘wings’ resulting in a teardrop shape<sup>28,29</sup> in order to reduce the curvature of the pore interface. A stalk opposes this rearrangement because it forces the trans-leaflets to remain largely parallel/horizontal<sup>30</sup>. The dashed lines in Figure S8b illustrate a fast decrease in curvature upon initial fusion pore opening. Here, the pre-existing curvature induced by HOPS (essentially a teardrop shape) is geometrically more compatible with a fusion pore than a stalk. This provides a relative free energy advantage for fusion pore formation.

In the absence of HOPS, the local curvature associated with nucleation of a fusion pore in flat membranes is so high that it seemingly becomes advantageous to form membrane defects near the transmembrane domains of the SNAREs (Fig. S8b). Such 'leaky' transitions are not observed in the presence of HOPS, probably because it lowers the threshold for fusion pore nucleation and thereby channels the reaction towards non-leaky fusion. We have also tested directly whether HOPS might render the fusion site prone to membrane rupture. To this end we placed the two probes such that pulling them together would locally disrupt the membrane near the stalk (see Fig. S8d). Enforcing such a membrane defect does not result in membrane rupture but the defect self-heals.

## Materials and Methods

### ***Strains and culture conditions***

All strains were grown in either in YPD (yeast extract, peptone, dextrose) containing 2% glucose in the presence or absence of G418, or in SC (synthetic dextrose) dropout media containing 2% glucose to select for auxotrophies. Strains used in this study can be found in Table S1. Primers used can be found in Table S2. Vam7-LL-2xFKBP12 contains a linker (LL) of 35 amino acids with the sequence SGGGGSGGGG SGGGGSGGGG SGGGGSGGGG GAAGG.

Genetic manipulations: Yeast transformations were carried out using the lithium acetate method. Gene deletions and tagging were performed as previously established<sup>31,32</sup>. Genome-tagging of Vam7 with 2xFKBP12 and LL-2xFKBP12 was performed starting from the plasmid pTK209, from which GFP was removed by double digestion with PacI and Ascl restriction enzymes and replaced by a 2xFKBP12 coding sequence carrying the same restriction sites. The 2xFKBP12 sequence was obtained by gene synthesis (BIOCAT) and cloned into a pUC57 vector. pRS415-TEFpr-FRB-GFP was obtained starting from a pRS416-S3-FRB-GFP vector (provided by C. Ungermann's group). The FRB-GFP coding frame was amplified by PCR using the primers reported above and cloned into the pRS415-TEFpr vector using HindIII and SacI restriction sites.

**Table S1: Yeast strains used in this study**

<b>Strain</b>	<b>Genotype</b>	<b>Reference</b>
BJ3505	MATa pep4::HIS3 prb1-Δ 1.6R lys2-208 trp1-Δ 101 ura3-52 gal2 can	<sup>33</sup>
DKY6281	MATα pho8::TRP1 leu2-3 leu2-112 lys2-801 suc2-Δ 9 trp1-Δ 901 ura3-52	<sup>34</sup>
BY4742	MATa his3-1 leu2-0 met15-0 ura3-0	Lab stock
BJ Vam3-myc	BJ3505; Vam3-His6(myc)2::URA	<sup>6</sup>
BJ Nyv1-HA	BJ3505; Nyv1-His6(HA)3::URA	<sup>6</sup>
BJ ypt7Δ	BJ3505; ypt7::G418	Lab stock
DKY ypt7Δ	DKY6281; ypt7::G418	Lab stock
BJ ypt7Δ Nyv1-HA	BJ3505 ypt7Δ; Nyv1-His6(HA)3::URA	This study
BJ ypt7Δ Vam3-myc	BJ3505 ypt7Δ; Vam3-His6(myc)2::URA	This study
BY tor1-1 Vam7-2xFKBP12	BY4742; Vam7-2xFKBP12::URA	This study
BY tor1-1 Vam7-2xFKBP12 Pfk1-FRB-GFP	BY4742; Vam7-2xFKBP12::URA ; Pfk1-FRB-GFP::G418	This study

BY tor1-1 Pfk1-FRB-GFP	BY4742; Pfk1-FRB-GFP::G418	This study
BY tor1-1 Vam7-LL-2xFKBP12	BY4742; Vam7-LL-2xFKBP12::URA	This study
BY tor1-1 Vam7-LL-2xFKBP12		
Pfk1-FRB-GFP	BY4742; Vam7-LL-2xFKBP12::URA ; Pfk1-FRB-GFP::G418	This study
BY tor1-1 Vam7-2xFKBP12 + FRB-GFP	BY4742; Vam7-2xFKBP12::URA ; pRS415-TEFpr-FRB-GFP (LEU)	This study
CUY2675 GAL-HOPS Vps41-TAP	MATa/alpha his3 $\Delta$ 200 leu2 $\Delta$ 0/leu2 $\Delta$ 0 lys2 $\Delta$ 0 met15 $\Delta$ 0/met15 $\Delta$ 0 trp1 $\Delta$ 63/trp1 $\Delta$ 63 ura3 $\Delta$ 0/ura3 $\Delta$ 0 VPS11pr::HIS3-GAL1pr VPS16::natNT2-GAL1pr VPS18::KanMX-GAL1pr-3HA VPS33::TRP1-GAL1pr VPS41::TRP-GAL1pr-TAP-URA3 VPS39::HIS3-GALpr	<sup>35</sup>
CUY3238 GAL-Vps33-16 Vps16-TAP	MATa his3 $\Delta$ 200 leu2 $\Delta$ 0 lys2 $\Delta$ 0 met15 $\Delta$ 0 trp1 $\Delta$ 63 ura3 $\Delta$ 0 VPS33::HIS3-GALpr Vps16::TRP-GAL1pr-TAP-URA3	<sup>35</sup>
CUY4307 GAL-Vps39-11 Vps39-TAP	MATa/alpha his3 $\Delta$ 200 leu2 $\Delta$ 0/leu2d0 lys2 $\Delta$ 0 met15 $\Delta$ 0/met15d0 trp1 $\Delta$ 63/trp1 $\Delta$ 63 ura3 $\Delta$ 0/ura3 $\Delta$ 0 VPS11pr::HIS3-GAL1pr VAM6pr::KanMX-GAL1pr VAM6::TAP-URA3	<sup>35</sup>
CUY4895 GAL-CORVET Vps8-TAP	MATa/alpha his3 $\Delta$ 200 leu2 $\Delta$ 0/leu2 $\Delta$ 0 lys2 $\Delta$ 0 met15 $\Delta$ 0/met15 $\Delta$ 0 trp1 $\Delta$ 63/trp1 $\Delta$ 63 ura3 $\Delta$ 0/ura3 $\Delta$ 0 VPS11pr::HIS3-GAL1pr VPS16::natNT2-GAL1pr VPS18::KanMX-GAL1pr-3HA VPS33::TRP1-GAL1pr VPS8::TRP-GAL1pr-TAP-URA3 VPS3::HIS3-GALpr	<sup>35</sup>
CUY8919 GAL-Vps33-TAP	MATa his3 $\Delta$ 200 leu2 $\Delta$ 0 lys2 $\Delta$ 0 met15 $\Delta$ 0 trp1 $\Delta$ 63 ura3 $\Delta$ 0 VPS33::HIS3-GALpr-TAP-URA3	<sup>35</sup>

**Table S2: Primers used for genetic manipulations**

Primer	Sequence
Fw Vam3-myc	ATTATAATAGTTGTGTGCATGGTGGTATTGCTTGCTGTATTAAGTTCCC ACCACCATCATCATCAC
Rv Vam3-myc	TAATCTCCTTAAACGCGCATTGAGCACAGACTTTCTGGTAGACCCACTA TAGGGAGACCGGCAGATC
Fw Nyv1-HA	ATTATACTATTTGTAAGTGCTGCTTTCATGTTTTTCTATCTGTGGTCCCA CCACCATCATCATCAC



mg/ml creatine kinase, 20 mM creatine phosphate, 500  $\mu$ M ATP, 500  $\mu$ M  $MgCl_2$ ) or of 600 nM rVam7 and 10 mg/ml BSA. Samples were incubated for 60 min at 27°C. In two-stage reactions, a second incubation of 15 at 27°C was added, with 200 nM of antibodies or 400 nM of purified HOPS subunits. In order to assay fusion, 1 ml of PS buffer was added, vacuoles were centrifuged (2 min, 20'000xg, 4°C) and resuspended in 500  $\mu$ l developing buffer (10 mM  $MgCl_2$ , 0.2% TX-100, 250 mM Tris-HCl pH 8.9, 1 mM p-nitrophenylphosphate). After 5 min at 27°C, the reactions were stopped with 500  $\mu$ l 1M glycine pH 11.5 and the OD was measured at 405 nm. Background activity of pro-Pho8 was assessed through a fusion sample kept on ice throughout the incubation period. The value of this sample was subtracted from the others.

### ***Lipid mixing assay***

Lipid mixing was assayed as described<sup>36</sup>. In brief, 30  $\mu$ g of unlabeled BJ3505 vacuoles and 6  $\mu$ g of rhodamine-labeled phosphoethanolamine DKY6281 vacuoles were mixed in 190  $\mu$ l of 0.3 mM  $MnCl_2$ , 75 mM KCl in PS buffer. Inhibitors were pre-warmed to 27°C before being adding to the tubes. Fusion reactions were started by adding 9.5  $\mu$ l of 20x ATP-regeneration system, yielding 0.125 mg/ml creatine kinase, 20 mM creatine phosphate, 0.5 mM ATP, 0.5 mM  $MgCl_2$ . 100  $\mu$ l were used to assay lipid mixing in a fluorescent plate reader at 27°C for 32 min. 80  $\mu$ l were incubated separately for 60 min and then assayed for content mixing by alkaline phosphatase developing buffer as described above.

### ***Immunoprecipitations***

Vacuoles from a 1 ml fusion reaction were pelleted (5 min, 6'000 xg, 4°C), solubilized for 10 min in lysis buffer (0.5% Triton X-100, 0.5 mM  $MnCl_2$ , 100 mM  $CaCl_2$ , 1 mM PMSF) and centrifuged for 10 min at 12'000 xg and 4°C. The supernatant was supplemented with 30  $\mu$ g of antibody and 25  $\mu$ l of protein-G sepharose and shaken for 60 min at 4°C. The beads were washed three times with lysis buffer and suspended in SDS sample buffer.

### ***Gel electrophoresis and Western blot***

Protein samples were dissolved in reducing sample buffer and heated to 95 °C for 5 minutes. The samples were run on either 10 % or 12.5 % polyacrylamide gels. The stacking gels were prepared as follows: 6 % acrylamide, 0.16 % bis-acrylamide, 0.1

M Tris pH 6.8, 0.1 % SDS, 0.1 % TEMED, 0.05 % ammonium persulfate. Running gels were: 10 % or 12.5 % acrylamide, 0.27 % or 0.34 % bis-acrylamide, 0.38 M Tris pH 8.8, 0.1 % SDS, 0.06 % TEMED, 0.06 % APS. The gels (10 cm/ 8 cm/ 1.5 mm) were run at constant current (20-30 mA). Proteins were blotted onto nitrocellulose membrane by the semidry method for 80 min at 400 mA. After incubation with the primary antibody overnight, signals were detected by secondary antibodies coupled to infrared dyes and detected on a LICOR Odyssey infrared laser scanner. The files were exported as TIFF and processed in adobe illustrator CS3. Band intensity was quantified using densitometry software supplied with the Odyssey Infrared Imager.

### ***FM4-64 staining***

Cells were inoculated from a pre-culture in stationary phase and grown overnight to logarithmic phase ( $OD_{600}$  between 0.2 and 0.8). After dilution to an  $OD_{600}$  of 0.2 in 1 ml culture, FM4-64 in DMSO was added to a final concentration of 10  $\mu$ M. Cells were stained for 1 h, followed by three washing steps in medium without stain (2 min, 3'000 xg) and a subsequent chase of 1 to 2 h in medium without stain, depending on the endocytotic capacity of the strain. The cells for microscopy were grown at 30°C. The temperature was kept constant during staining and visualization. Care was taken to analyze cells immediately after their removal from the culture tube.

### ***Affinity purification of antibodies***

Antibodies against Vam3, Nyv1, Vam7, Vps39 and Ypt7 had been raised by injecting purified recombinant hydrophilic parts of these proteins into rabbits. Antibodies were purified from sera. Sera were first heated for 30 minutes at 56°C to inactivate the complement system, diluted 1:1 in PBS and filtered through 0.2 $\mu$  membranes before being passed onto an activated CH-sepharose 4B column (GE Healthcare Life Sciences 17-0430-01), which had been coupled with the recombinant protein of interest, according to the instructions of the manufacturer. The column was washed with 10 bed volumes of PBS at 4°C. The antibodies were eluted with 0.2 M glycine-HCl pH 2.5, 4°C, using a peristaltic pump. Eluted fractions were collected on ice in 1,5 ml tubes containing 150  $\mu$ l of 1 M Tris pH 8.8 in order to neutralize the samples immediately. Protein concentration in the sample was determined by Bradford assay using BSA as a standard. Fractions of interest were pooled, transferred into PS buffer (10 mM PIPES-KOH pH 6.8, 200 mM sorbitol) containing 150 mM KCl by repeated dilution and re-concentration in Amicom®Ultra-15 30K ultrafiltration

devices (Millipore). The antibodies were finally concentrated to 1-3 mg/ml, aliquoted, flashed frozen in liquid nitrogen and kept at -20°C.

### ***Papain digestion and F<sub>ab</sub> fragment purification***

Antibody digestion with papain was described previously<sup>38</sup>. Briefly, 10 mg affinity-purified IgG were solubilized in 1 ml buffer A (150 mM NaCl, 1 mM EDTA, 25 mM mercaptoethanol, 10 mM NaP<sub>i</sub> pH 7.3), followed by addition of 0.1 mg papain and incubation for 3 h at 37° C. 30 mM iodoacetamide was added to inhibit papain (15 min at 37° C). Afterwards, the sample was chilled to 4°C and loaded on a protein A agarose column (Pharmacia; 1.5 ml volume), which was equilibrated before with buffer B (100 mM KP<sub>i</sub>, pH 8.0). The F<sub>ab</sub>-containing flow-through was dialyzed against H<sub>2</sub>O and concentrated by ultrafiltration through 30 kDa cutoff membranes (Millipore).

### ***Purification of rVam7***

Plasmid pGEX-KT::Vam7 (kind gift from A. Merz, Seattle) was expressed in Rosetta 2 (DE3) (Novagen). Bacteria were grown in 2 l LB with 100 µg/ml ampicillin and 25 µg/ml chloramphenicol to OD<sub>600</sub>=1, induced with 1 mM IPTG, 30°C for 4 h. Cells were harvested and washed with PBSEEG (2 mM EDTA, 1 mM EGTA, 2 mM DTT, 1 mM PMSF in 1X PBS). The pellet was frozen in liquid nitrogen and stored at -80°C. For purification the sample was thawed, resuspended in 40 ml PBSEEG, sonicated (2 x 1 min on ice with maximal intensity), centrifuged (TI-60 rotor, 64'000 x g, 30 min, 4°C) and the supernatant was incubated with 2-3 ml glutathion-sepharose 4B (GE Healthcare, 17-0756-01) under gentle rotation overnight, at 4°C and washed 3-4 x with PBSEEG. The resin was poured into a 10 ml polypropylene column (Thermo scientific N°2994), washed with 10 bed volumes of thrombin cleavage buffer (50 mM Tris-HCl pH 8.0, 100 mM NaCl, 2.5 mM CaCl<sub>2</sub>, 0.1 % β-mercaptoethanol) at room temperature. 200 Units of thrombin (Sigma T-1063, 1000 U, dissolved in 0.5 ml thrombin cleavage buffer and 0.5 ml glycerol, aliquots had been kept at -20°C) were then added directly onto the column, the column was closed on both ends and incubated for 30 minutes at room temperature with end over end rotation. A second column with 1 ml p-aminobenzamidine agarose (Sigma A-8332, 5 ml) was washed with 20 ml thrombin cleavage buffer. The glutathione sepharose column was eluted with thrombin cleavage buffer directly onto this second column. Fractions of the flow-through were collected at the bottom of the second column. Protein levels were measured and fractions of interest were pooled. Eluted

protein was transferred into PS buffer (10 mM PIPES-KOH pH 6.8, 200 mM sorbitol) containing 150 mM KCl by repeated dilution and ultrafiltration in Amicon Ultra-15 30K (Millipore), finally concentrated to 3 mg/ml, aliquoted, flash-frozen in liquid nitrogen and kept at -20°C.

### ***Purification of HOPS, HOPS subcomplexes and CORVET***

These complexes were purified via the TAP protocol, as previously described (Ostrowicz, Brocker et al., 2010). In brief, yeast cell lysates were prepared from 500 OD<sub>600</sub> equivalents of cells by thoroughly vortexing cells in lysis buffer [50 mM HEPES/KOH, pH 7.4, 300 mM NaCl, 0.15% NP-40 (Igepal CA-630; Sigma-Aldrich), 2 mM MgCl<sub>2</sub>, 1 mM DTT, 1 mM phenylmethylsulphonyl fluoride (PMSF) and 1xFY protease inhibitor mix (Serva)] together with glass beads in a Disrupter Genie for 10 min at 2°C, followed by centrifugation at 20'000 xg at 4°C. The supernatant was centrifuged for 60 min at 100'000 xg and the cleared lysate loaded onto 25 µl of prewashed IgG beads. After 1 h of incubation at 4°C, the beads were washed 3 times with 1 ml lysis buffer containing 0.5 mM DTT, but lacking protease inhibitors. Bound proteins were eluted by TEV protease treatment for 1 h at 16°C. TEV eluates were either analyzed by SDS-PAGE and Coomassie staining or loaded onto 25 µl of prewashed calmodulin-sepharose beads, and incubated for 1 h at 4°C. The beads were washed 3 times with 1 ml lysis buffer, bound proteins were eluted by incubation with 20 mM EGTA in lysis buffer for 20 min at 30°C, analyzed by SDS-PAGE and Coomassie staining and kept in small aliquots at -20°C. Aliquots were thawed and the proteins transferred into lysis buffer without DTT and NP-40 by repeated dilution and ultrafiltration (4°C) in Amicon Ultra-15 30K (Millipore). Re-concentrated proteins were used immediately for the experiment and not re-frozen.

### ***Rapamycin-induced protein re-localisation***

Cells were grown in YPD over night at 30°C to early logarithmic phase. Cells were diluted to OD<sub>600</sub>=0.2 for staining with 5 µM FM4-64 and then incubated with rapamycin (10 µM) before image acquisition.

### ***Statistics for biological experiments***

When data was averaged, the samples stem from independent experiments with independent preparations of vacuoles or cells, i.e. they represent biological replicates. The number of replicates is indicated in all figures as *n*, the variation of

their values is characterized by the standard deviation (s. d.). Significance of differences has been evaluated through Student's t-test. Differences are only mentioned as such and interpreted if  $p < 0.005$ .

## **Molecular dynamics**

### ***Simulation model and settings***

The molecular dynamics simulations were performed with the GROMACS simulation package<sup>39</sup>, version 4.5.7. We used the MARTINI coarse-grained model<sup>40,41</sup> to simulate the lipids, amino acids and solvent. In all simulations, the system was coupled to a constant temperature bath using the 'V-rescale' algorithm with a relaxation time of 1.0 ps. All simulations were performed at a temperature of 293 K. Periodic boundary conditions were applied to simulate bulk behavior. The time step used in the simulation was 20 fs. The dielectric constant in the simulations was  $\epsilon_r = 15$ . The neighbor-list was updated every 10 simulation steps. The pressure was weakly coupled<sup>42</sup> to 1 bar with a relaxation time of 1.0 ps. Here, only the z-dimension was independently coupled to the pressure bath because the x and y-dimension of the simulation box were conserved (see *Membrane simulation setups*).

### ***Modeling the vacuolar SNARE complex***

The vacuole SNARE complex was modeled using the MARTINI model for proteins<sup>40</sup>, which qualitatively captures the chemical nature of each individual amino acid and includes the secondary structure. For NYV1 the modeled sequence is “IGDATEDQIKDVIQIMNDNIDKFLERQERVSLLDKTSQNLNSSSNKFRRKAVNIKEIMWW[QKVKNI]ITLLTFTIILFVSAAFMFFYLW”, for VAM3: “TIIHQERSQQIGRIHTAVQEVNAIFHQLGSLVKEQGEQVTTIDENISHLHDNMQNANKQLTRA[DAQHQRDRNK]CGKVTLIIIVVCMVLLAVLS”, for VTI1: “IDDDQRQQLLSNHAILQKSGDRLKDASRIANETEGIGSQIMMDLRSQRETLENARQTLFQADSYVDKSIKTLKTMTR[RLVANK]FISYAIIVLILLILLVLFKFK”, and for VAM7 “MQMVRDQEQELVALHRIQAQRGLALEMNEELQTQNELLTALEDDVDNTGRRLLQIANKKARHF”. Here, the brackets [] depict the defined juxta-membrane (linker) regions. The resolved and previously simulated structure<sup>42</sup> of the neuronal SNARE complex was used as a template structure for the vacuolar SNARE complex. To this aim, we applied an external field, using a self-modified version of Gromacs, to drive the structure of the vacuole SNARE complex toward the known structure of the neuronal SNARE

complex based on the known alignment. All residues are defined alpha-helical except for the defined SNARE linkers. The linkers are either modeled as a random coil '~' (in case of unstructured) or alpha helical 'H' (in case of structured). We modeled all of the three SNARE linkers as being structured because such a scenario maximizes the force which a partly-assembled SNARE complex, by itself, can exert on the formed stalk.

### **Membrane simulation setups**

In total three different 'HOPS' systems were simulated (Tab. S3).

**Table S3: Overview of the different simulation systems.**

System	#SNARE compl.	#POPC	#POPE	#Solvent	Dimension (nm <sup>3</sup> )	t <sub>eq</sub> (μs)	Used in Fig.:
1	3	10'158	6'771	663'000	48x64x37	1	4b,S8
2	1	10'983	-	400'000	48x40x33	1	4a,S9b,S10
3*	1	13'621	-	500'000	67x40x40	2	4a,S9b

\*For studying the fusion pore the system was made slightly larger in order to prevent a too close distance between the fusion pore and the free membrane edges (see the description below).

It is important to emphasize that the two opposing membranes must be able to freely adopt their (local) separation distance in order to realistically mimic a scenario where two vacuoles fuse. To this aim, we cut the periodicity of the membrane along the x-dimension (thus preventing that solvent is 'trapped' in the space between the two opposing leaflets). The latter creates four free membrane edges (e.g., see Fig. S8) which facilitate rapid flip-flop between the leaflets and thereby ensure that the spontaneous curvature of the membrane vanishes when the membrane is bent (preventing finite size effects). Furthermore, the ability to freely adapt the area of the membrane ensures that the membrane minimizes its shape under tension-less conditions in the presence of HOPS and thus the work performed by HOPS is only determined by membrane bending energy. Finally, to prevent that the large line tension of the free membrane edges would strongly deform the simulation box (it prefers to minimize the y-dimension while maximizing the x-dimension) the x- and y dimension of the simulation box were kept constant. Hence, pressure coupling along these dimensions is redundant for a membrane cut in one dimension because the

membrane area can independently adjust with respect to the (corresponding) area of the simulation box (the system is isotropic).

### **Model and setup of the HOPS simulations**

In our simulations, 'soluble' HOPS is modeled by a soft harmonic repulsive potential ( $K_{\text{force}} = 50 \text{ kJ nm}^{-2} \text{ mol}^{-1}$ ). The 'attractive' HOPS is modeled by the potential function,  $V(d) = K_{\text{force}} d^2 (d^2 - C)$ , where  $V(d)$  is the potential energy as a function of the penetration depth  $d$ , i.e. the distance beyond the surface of 'HOPS'. Here,  $K_{\text{force}}$  and  $C$  (the width of the well) are set to  $K_{\text{force}} = 20 \text{ kJ nm}^{-2} \text{ mol}^{-1}$  and  $C = 0.4 \text{ nm}^2$ . Because the additional presence of attractions reduces the apparent radius of HOPS we compensated for this by slightly increasing its radius (7.4 nm versus 7.0 nm). The 'HOPS' potential only acted on the carbon tails and glycerol parts of the lipids. To mimic a SNARE complex which is slightly embedded by HOPS<sup>14</sup> we modeled a slight overlap between HOPS and the SNARE complex, i.e. the SNARE complex is located within HOPS about 2 nm away from its surface (see Figs. S8, S10). In reality, the depletion of solvent interactions upon binding will be compensated by competitive interactions with the binding pocket of HOPS. In our model, solvent was allowed to freely enter and pass 'HOPS' in order to conserve ongoing interactions within the coiled-coil complex of the SNAREs. The main advantage of modeling HOPS by an effective potential is that this allows direct quantification of the work which HOPS must perform to conserve the corresponding membrane shape of minimal free energy. The HOPS simulations were setup via the slow growth method, i.e., the radius of HOPS was gradually increased from 0 to the target radius over 80ns. During this procedure, the SNARE complex was restrained by restraining only a single bead within the SNARE complex (the backbone bead of residue GLY218 within VAM3) via a harmonic potential ( $K_{\text{force}} = 1000 \text{ kJ nm}^{-2} \text{ mol}^{-1}$ ). After equilibrium was reached – equilibrium was characterized by the pressure (bending work) and the resultant force on HOPS - we restrained 15 additional backbone atoms within VAM3 (GLY218 - ASP232) to simulate a torsional restraining effect of the binding pocket on the SNARE complex.

Finally, the stalk in all of the setups is generated by applying an external field. Here, we applied a harmonic potential ( $50 \text{ kJ nm}^{-2} \text{ mol}^{-1}$ ) to induce a cylindrically shaped 'void' of 1.0 nm radius in the solvent layer between the bilayers. The hydrophobic nature of the void attracts the lipid tails in the adjacent leaflets and results in the formation of a stalk. Notable, this whole process occurs on a timescale of a few

nanoseconds only. The external potential is removed prior to subsequent equilibration and introduction of the HOPS sphere.

### **Free energy of fusion and SNARE forces**

We performed two different types of so-called umbrella sampling protocols (Tab. S4).

**Table S4: Overview of the two different umbrella sampling protocols**

Protocol	Goal	Reaction coordinate	System type (see Table 3)
A	How does HOPS binding affect the free energy landscape of fusion pore opening?	Probe to probe distance (stalk thickness).	1
B	How does HOPS binding affect the force that the bound SNARE complex exerts on a fusion intermediate.	Distance between the C-termini of Nyv1 and Vam3.	2

In protocol A, we pull two hydrophilic 'beads' (probes) through the stalk center in order to estimate the free energy required to open the fusion pore. Each probe is comprised of 8 clustered solvent beads. The "stalk thickness" is defined by the distance between the two probes. The rationale is to bring the system close to the nucleation barrier until that barrier can be crossed spontaneously within the simulation time scales. The work required to enforce nucleation provides an estimate of the height of the barrier. For more detailed information see our previous work<sup>26</sup>.

In protocol B, we study how HOPS binding alters the force that the C-termini of Nyv1 and Vam3 exert on the stalk intermediate. We rationalize such an effect from the relative change in work required to *slightly* pull the SNARE C-termini (Nyv1 and Vam3) in closer proximity in the presence or absence of HOPS. *Slightly* implies that we only indent/squeeze the stalk such that the stalk will recover if no active pulling force is applied anymore (thermodynamically reversible).

To derive the associated free energies in both of these protocols, we applied umbrella simulation techniques ( $K_{\text{force}} = 1000 \text{ kJ nm}^{-2}\text{mol}^{-1}$ ) in combination with the weighted histogram method. We generated independent states along the reaction coordinate (50 for protocol A, 15 for protocol B) by performing a stirred molecular

dynamics simulation over the entire reaction coordinate (pull rate:  $-5 \times 10^{-5}$  nm/ps) in a pre-equilibrated system. Equilibrium was characterized by the pressure (bending work) and the resultant force on HOPS. For protocol A, a separate, independent stirred MD run must be performed for each different system (e.g., the attractive HOPS case) because the generated states will embed information about the nature of the barrier. The umbrella simulations were performed after the systems were equilibrated for  $\sim 1.6$   $\mu$ s, i.e., the last snapshot was used for a stirred MD simulation, from which the different umbrella windows were generated. Equilibrium was characterized by the pressure (bending work) and the resultant force on HOPS. Each umbrella window was simulated over an effective time of 400-600 ns to obtain overlapping distributions from which the total free energy profile was constructed. We discarded the first 40 ns of the simulation to ensure equilibration of the measured biased force. All of the free energy profiles and the error bars herein were obtained by using the Weighted Histogram Analysis Method (WHAM) in combination with the Bayesian bootstrapping method<sup>43</sup>. The bootstrapping method exploits the WHAM equations to reconstruct a large multiple of free energy profiles from re-sampled bootstrap histograms. The errors within the final free energy profile are estimated from the statistical fluctuations herein. Each re-sampled histogram of the biased force is reconstructed from the data which comprise the original histogram (an umbrella window) by random selection with replacement. This resampling procedure respects the (on the fly estimated) integrated autocorrelation time within the biasing force and adds an additional random weight to the histogram within the WHAM equations (Bayesian bootstrapping). An excellent detailed description of this procedure has been given<sup>43</sup>.

### *Bending energy and force*

The bending work is calculated from the (partial) pressure which the membrane exerts on the surface of HOPS. In mechanical equilibrium, the equilibrium work ( $W_{eq}$ ), which HOPS must perform to conserve the membrane shape of minimal free energy, equals the exerted pressure ( $P$ ) times the volume ( $V$ ) of HOPS. This relationship reduces to  $W_{eq} = 1/3 \sum F \cdot r$ , where  $\sum F \cdot r$  is the summation over all (normal) forces  $F$  acting on the surface of HOPS times the radius  $r$  of HOPS. For a purely repulsive sphere this will approximate the concomitant bending energy of the adopted shape. The obtained values of 100-250  $k_B T$  for the HOPS-hemifusion complex are about a factor of two larger than predicted by the Helfrich continuum

model (see Fig. S9). The reason for this is that HOPS bends the membrane by actively pressing against the membrane surface (indentation). This additional stress term (e.g., thinning of the membrane) is not included within the Hamiltonian of the continuum model. This missing term, however, equally contributes to the total surface free energy (a factor of two) because bending and indentation directly compete with each other and must therefore compensate each other at mechanical equilibrium. This principle is analogous to the principle of two joined springs which must perform the same amount of work during stretching irrespective of the difference in stiffness of the springs. The peristaltic force ( $f_d$ ) on HOPS (see Fig. S9) is calculated from projecting the resultant force on HOPS (a 3-vector) on the vector connecting the center of HOPS with the stalk center. Here, the stalk center is defined as the geometrical center between the C-terminus of NYV1 and VAM3. Finally, the average values of bending work and  $f_d$  are obtained by averaging over 1 - 2  $\mu$ s equilibrium simulations. The error in the average value is obtained by block averaging.

### ***Continuum model***

Continuum models were performed by minimizing the Helfrich hamiltonian within the de Monge representation  $z(x,y)$  subjected to two constraints: (i) The inter-membrane constraint (a stalk or partly-assembled SNARE complex) and, (ii) a solid sphere (HOPS). The membrane was described by a *discretized* sheet consisting of 100 grid elements in the y, and 200 in the x dimension. For reasons of symmetry we only model a quarter of the actual system and recover the full surface free energy by multiplication with a factor of 4 (for the projected area by a factor of 2). Reflecting boundary conditions were used in the y-dimension (the symmetry axis), periodic in the x-dimension. The actual membrane contact surface in vacuole fusion is of microscopic dimension<sup>19,44,45</sup>, indicating that a large multiple of constraints must be present and that the membrane is not 'free standing' even over large distances. All dimensions are based on the positions of the C4 lipid tail beads (the mid-plane of the membrane) within the MD simulations. Finally, HOPS embeds the SNARE complex non-symmetrically<sup>14</sup> and will therefore induce torque. Torque (a three body force) does not occur when the distance (d) between the center of HOPS and the stalk (the two constraints) is used as a reaction coordinate but can be additionally derived/constructed by scaling the here-presented force ( $f_d$ ) with a  $\sin(\theta)$  term.

The Hamiltonian for each surface element,  $F_{\text{total}}$ , is given by  $F_{\text{bending}} + F_{\text{constraint}} + F_{\text{HOPS}}$ , with  $F_{\text{bending}}$  being the Helfrich bending energy,  $F_{\text{constraint}}$  the energy of the inter-membrane constraint (a stalk, fusion pore or partly-assembled SNARE complex) and  $F_{\text{HOPS}}$  the energy of the HOPS' sphere.  $F_{\text{bending}}$  is given by  $2\kappa H^2$  with  $H$  being the mean curvature, and  $\kappa$  the bending modulus ( $24 k_B T$ , see citation<sup>9</sup>). The constraint  $F_{\text{constraint}}$  is modeled by a set of stiff springs which restraints the membrane at a height of  $z_{\text{equ}} = 2$  nm and which imposes a circular 'stalk' region with a radius of  $d_{\text{stalk}} = 2$  nm.  $F_{\text{constraint}}$  depends on the distance  $d$  between a surface element and the center of the 'stalk' region, and the height of the membrane  $z$ .  $F_{\text{constraint}} = 0$  if  $d > 2$  nm and  $1/2k_{\text{stalk}}(z-z_{\text{eq}})^2(d-d_{\text{stalk}})$  otherwise, with  $k_{\text{stalk}}$  being the force constant ( $k_{\text{stalk}} = 100 k_B T/\text{nm}^5$ ). Here, the term  $(d-d_{\text{stalk}})$  ensures a smooth (differentiable) transition of the 'stalk' region. HOPS was modeled as a sphere with a diameter  $D_H$ . The center of the sphere is located within the  $x,y$  plane at  $z=0$ . Surface elements overlapping with the HOPS sphere experience an harmonic repulsion,  $F_{\text{HOPS}} = 1/2k_{\text{HOPS}}(2r-D_H)^2$  if  $2r < D_H$  and  $F_{\text{HOPS}} = 0$  otherwise, with  $r$  being the distance of a surface element from the center of the sphere. The force constant  $k_{\text{HOPS}}$  was chosen to be  $100 k_B T/\text{nm}^4$ . The example of a (moderately) attractive HOPS was modeled using  $F_{\text{HOPS}} = K_{\text{HOPS}}d^2(d^2-C)$  with  $C = 0.5 \text{ nm}^2$ , and  $K_{\text{HOPS}} = 20 k_B T/\text{nm}^6$ . Finally, the total surface free energy  $\int F_{\text{total}} dA$  was minimized using an over-damped deterministic minimization scheme.

### ***Code availability***

The molecular dynamics simulations were performed with a self-modified version of the open source software Gromacs-4.5.5. The implementation of the here-used HOPS potentials is described in detail in the SI. After publication, the code will be made publically available via [www.stocs.net](http://www.stocs.net)

## Supplementary References:

1. Sato, T. K., Rehling, P., Peterson, M. R. & Emr, S. D. Class C Vps protein complex regulates vacuolar SNARE pairing and is required for vesicle docking/fusion. *Mol Cell* **6**, 661–671 (2000).
2. Orr, A., Song, H., Rusin, S. F., Kettenbach, A. N. & Wickner, W. HOPS catalyzes the interdependent assembly of each vacuolar SNARE into a SNARE complex. *Mol. Biol. Cell* **28**, 975–983 (2017).
3. Krämer, L. & Ungermann, C. HOPS drives vacuole fusion by binding the vacuolar SNARE complex and the Vam7 PX domain via two distinct sites. *Mol. Biol. Cell* **22**, 2601–2611 (2011).
4. Baker, R. W. *et al.* A direct role for the Sec1/Munc18-family protein Vps33 as a template for SNARE assembly. *Science* **349**, 1111–1114 (2015).
5. Lobingier, B. T. & Merz, A. J. Sec1/Munc18 protein Vps33 binds to SNARE domains and the quaternary SNARE complex. *Mol. Biol. Cell* **23**, 4611–4622 (2012).
6. Pieren, M., Schmidt, A. & Mayer, A. The SM protein Vps33 and the t-SNARE H(abc) domain promote fusion pore opening. *Nat Struct Mol Biol* **17**, 710–717 (2010).
7. Zick, M. & Wickner, W. T. A distinct tethering step is vital for vacuole membrane fusion. *elife* **3**, e03251 (2014).
8. Zick, M., Orr, A., Schwartz, M. L., Merz, A. J. & Wickner, W. T. Sec17 can trigger fusion of trans-SNARE paired membranes without Sec18. *PNAS* **112**, E2290–E2297 (2015).
9. Song, H., Orr, A., Duan, M., Merz, A. J. & Wickner, W. Sec17/Sec18 act twice, enhancing membrane fusion and then disassembling cis-SNARE complexes. *elife* **6**, 1111 (2017).
10. Schwartz, M. L. & Merz, A. J. Capture and release of partially zipped trans-SNARE complexes on intact organelles. *J Cell Biol* **185**, 535–549 (2009).
11. Mayer, A., Wickner, W. & Haas, A. Sec18p (NSF)-driven release of Sec17p (alpha-SNAP) can precede docking and fusion of yeast vacuoles. *Cell* **85**, 83–94 (1996).
12. Wang, L., Ungermann, C. & Wickner, W. The docking of primed vacuoles can be reversibly arrested by excess Sec17p (alpha-SNAP). *PNAS* **275**, 22862–22867 (2000).
13. Zhao, M. *et al.* Mechanistic insights into the recycling machine of the SNARE complex. *Nature* (2015). doi:10.1038/nature14148
14. Kuhlee, A., Raunser, S. & Ungermann, C. Functional homologies in vesicle tethering. *FEBS Lett* **589**, 2487–2497 (2015).
15. Bröcker, C. *et al.* Molecular architecture of the multisubunit homotypic fusion and vacuole protein sorting (HOPS) tethering complex. *PNAS* **109**, 1991–1996 (2012).
16. Martens, S., Kozlov, M. M. & McMahon, H. T. How synaptotagmin promotes membrane fusion. *Science* **316**, 1205–1208 (2007).
17. Hernandez, J. M., Kreutzberger, A. J. B., Kiessling, V., Tamm, L. K. & Jahn, R. Variable cooperativity in SNARE-mediated membrane fusion. *PNAS* **111**, 12037–12042 (2014).
18. Mattie, S., McNally, E. K., Karim, M. A., Vali, H. & Brett, C. L. How and why intraluminal membrane fragments form during vacuolar lysosome fusion. *Mol. Biol. Cell* **28**, 309–321 (2017).
19. Wang, L., Merz, A. J., Collins, K. M. & Wickner, W. Hierarchy of protein assembly at the vertex ring domain for yeast vacuole docking and fusion. *J Cell Biol* **160**, 365–374 (2003).

20. Gao, Y. *et al.* Single reconstituted neuronal SNARE complexes zipper in three distinct stages. *Science* **337**, 1340–1343 (2012).
21. Orr, A., Wickner, W., Rusin, S. F., Kettenbach, A. N. & Zick, M. Yeast vacuolar HOPS, regulated by its kinase, exploits affinities for acidic lipids and Rab:GTP for membrane binding and to catalyze tethering and fusion. *Mol. Biol. Cell* **26**, 305–315 (2015).
22. Lürick, A. *et al.* Multivalent Rab interactions determine tether-mediated membrane fusion. *Mol. Biol. Cell* mbc.E16–11–0764 (2016).  
doi:10.1091/mbc.E16-11-0764
23. Stein, A., Weber, G., Wahl, M. C. & Jahn, R. Helical extension of the neuronal SNARE complex into the membrane. *Nature* **460**, 525–528 (2009).
24. Zorman, S. *et al.* Common intermediates and kinetics, but different energetics, in the assembly of SNARE proteins. *elife* **3**, e03348–e03348 (2013).
25. Zhang, X. *et al.* Stability, folding dynamics, and long-range conformational transition of the synaptic t-SNARE complex. *Proc. Natl. Acad. Sci. U.S.A.* **113**, E8031–E8040 (2016).
26. Risselada, H. J., Bubnis, G. & Grubmüller, H. Expansion of the fusion stalk and its implication for biological membrane fusion. **111**, 11043–11048 (2014).
27. Hickey, C. M. & Wickner, W. HOPS initiates vacuole docking by tethering membranes before trans-SNARE complex assembly. *Mol. Biol. Cell* **21**, 2297–2305 (2010).
28. Ryham, R. J., Ward, M. A. & Cohen, F. S. Teardrop shapes minimize bending energy of fusion pores connecting planar bilayers. *Phys. Rev. E* **88**, 693 (2013).
29. Jackson, M. B. Minimum Membrane Bending Energies of Fusion Pores. *J Membr Biol* **231**, 101–115 (2009).
30. Kozlovsky, Y., Efrat, A., Siegel, D. P., Siegel, D. A. & Kozlov, M. M. Stalk phase formation: effects of dehydration and saddle splay modulus. *Biophys J* **87**, 2508–2521 (2004).
31. Janke, C. *et al.* A versatile toolbox for PCR-based tagging of yeast genes: new fluorescent proteins, more markers and promoter substitution cassettes. *Yeast* **21**, 947–962 (2004).
32. Longtine, M. S. *et al.* Additional modules for versatile and economical PCR-based gene deletion and modification in *Saccharomyces cerevisiae*. *Yeast* **14**, 953–961 (1998).
33. Jones, E. W., Zubenko, G. S. & Parker, R. R. PEP4 gene function is required for expression of several vacuolar hydrolases in *Saccharomyces cerevisiae*. *Genetics* **102**, 665–677 (1982).
34. Haas, A., Conradt, B. & Wickner, W. G-protein ligands inhibit in vitro reactions of vacuole inheritance. *J Cell Biol* **126**, 87–97 (1994).
35. Ostrowicz, C. W. *et al.* Defined subunit arrangement and rab interactions are required for functionality of the HOPS tethering complex. *Traffic* **11**, 1334–1346 (2010).
36. Reese, C., Heise, F. & Mayer, A. Trans-SNARE pairing can precede a hemifusion intermediate in intracellular membrane fusion. *Nature* **436**, 410–414 (2005).
37. Kuznetsova, I. M., Turoverov, K. K. & Uversky, V. N. What macromolecular crowding can do to a protein. *Int J Mol Sci* **15**, 23090–23140 (2014).
38. Mage, M. G. in *Immunochemical Techniques, Part A* **70**, 142–150 (Elsevier, 1980).
39. Hess, B., Kutzner, C., van der Spoel, D. & Lindahl, E. GROMACS 4: Algorithms for Highly Efficient, Load-Balanced, and Scalable Molecular

- Simulation. *J Chem Theory Comput* **4**, 435–447 (2008).
40. Monticelli, L. *et al.* The MARTINI Coarse-Grained Force Field: Extension to Proteins. *J Chem Theory Comput* **4**, 819–834 (2008).
  41. Marrink, S. J., Risselada, H. J., Yefimov, S., Tieleman, D. P. & de Vries, A. H. The MARTINI force field: coarse grained model for biomolecular simulations. *The journal of physical chemistry B* **111**, 7812–7824 (2007).
  42. Risselada, H. J., Kutzner, C. & Grubmüller, H. Caught in the act: visualization of SNARE-mediated fusion events in molecular detail. *Chembiochem* **12**, 1049–1055 (2011).
  43. Hub, J. S., De Groot, B. L. & van der Spoel, D. g\_wham—A Free Weighted Histogram Analysis Implementation Including Robust Error and Autocorrelation Estimates. *J Chem Theory Comput* **6**, 3713–3720 (2010).
  44. Mayer, A. & Wickner, W. Docking of yeast vacuoles is catalyzed by the Ras-like GTPase Ypt7p after symmetric priming by Sec18p (NSF). *J Cell Biol* **136**, 307–317 (1997).
  45. Karunakaran, S., Sasser, T., Rajalekshmi, S. & Fratti, R. A. SNAREs, HOPS, and regulatory lipids control the dynamics of vacuolar actin during homotypic fusion. *J Cell Sci* (2012). doi:10.1242/jcs.091900
  46. Merz, A. J. & Wickner, W. T. Resolution of organelle docking and fusion kinetics in a cell-free assay. **101**, 11548–11553 (2004).
  47. D'Agostino, M., Risselada, H. J. & Mayer, A. Steric hindrance of SNARE transmembrane domain organization impairs the hemifusion-to-fusion transition. *EMBO Rep* **17**, 1590–1608 (2016).
  48. Pieren, M., Desfougères, Y., Michailat, L., Schmidt, A. & Mayer, A. Vacuolar SNARE protein transmembrane domains serve as nonspecific membrane anchors with unequal roles in lipid mixing. *J. Biol. Chem.* **290**, 12821–12832 (2015).

## Supplementary Figures:

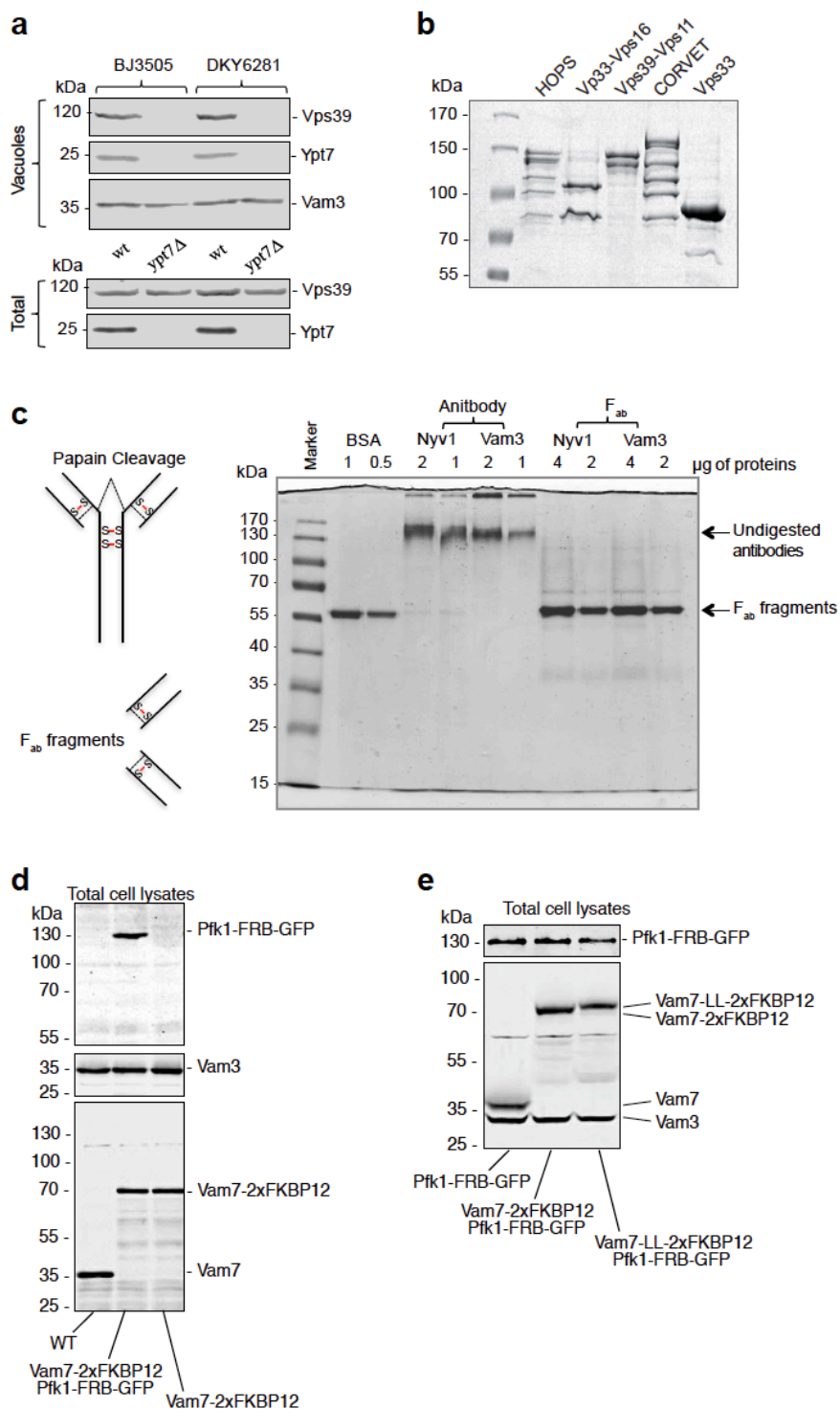


### Figure S1: Reagents.

**a**, HOPS is lacking on *ypt7* $\Delta$  vacuoles. HOPS and Ypt7 content of total cell extracts and purified vacuoles from wildtype and *ypt7* $\Delta$  mutants in BJ3505 and DKY6281 cells, representing the background strains used for the content mixing assay. **b**, Purified HOPS, HOPS subcomplexes and CORVET. The complexes used for the in

vitro experiments were analyzed by SDS-PAGE and Coomassie staining. **c**, Production of F<sub>ab</sub> fragments from polyclonal antibodies to Vam3 and Nyv1. Schematic view of papain cleavage sites for F<sub>ab</sub> fragment generation on the left. Affinity-purified antibodies and F<sub>ab</sub> fragments extracted after papain digestion were analyzed by non-reducing SDS-PAGE and Coomassie staining. **d**, Expression of FKBP and FRB fusion proteins. Total cell extracts were prepared from 0.1 OD<sub>600nm</sub> units of logarithmic cultures of yeast strains expressing Vam7-2xFKBP12 and/or Pfk1-FRB-GFP. Proteins were analyzed by SDS-PAGE and Western Blotting against Vam7, Vam3 and GFP. **e**, Same as in d, but for cells expressing Vam7-LL-2xFKBP12, containing the 35 aa linker (LL).

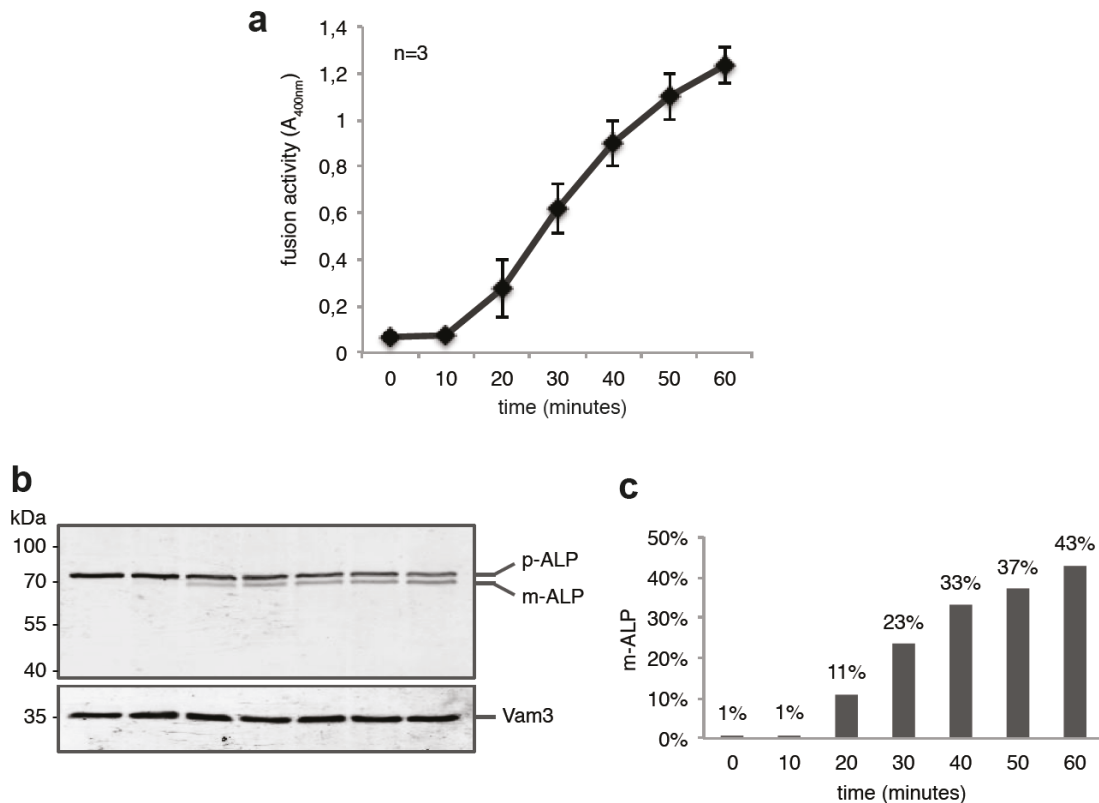


**Figure S2: Kinetics and efficiency of in vitro vacuole fusion, measured by content mixing.**

Vacuoles are prepared from two different strains, which contain either the soluble 45 kDa maturase Pep4 (contained in DKY6281) or the pro-alkaline phosphatase p-ALP (contained in BJ3505). Formation of a sufficiently large fusion pore allows Pep4 to transfer into the p-ALP containing fusion partner, leading to proteolytic cleavage of its pro-sequence and activation of the enzyme (m-ALP). This activity is measured as a readout for fusion. Note that proteolytic maturation of p-ALP is fast and not limiting for the development of the content mixing signal<sup>46</sup>. **a**, Standard fusion reactions have been started. At the indicated time points, aliquots were withdrawn and set on ice. At the end of the 60 min period, m-ALP activity was determined for all samples. Means  $\pm$  s.d. are shown.  $n=3$ . **b**, Aliquots from the same reaction were TCA-precipitated and analyzed by SDS-PAGE and Western blotting against ALP and Vam3. Signals were detected on a LICOR infrared scanner. Note that after one round of fusion, only a maximum of 50% of p-ALP can be matured, because half of the fusion events in the suspension will occur between like vacuoles (i.e. Pep4/Pep4 or p-ALP/p-ALP) and will not produce a signal **c**, The bands for m-ALP from **b** were quantified by densitometry.

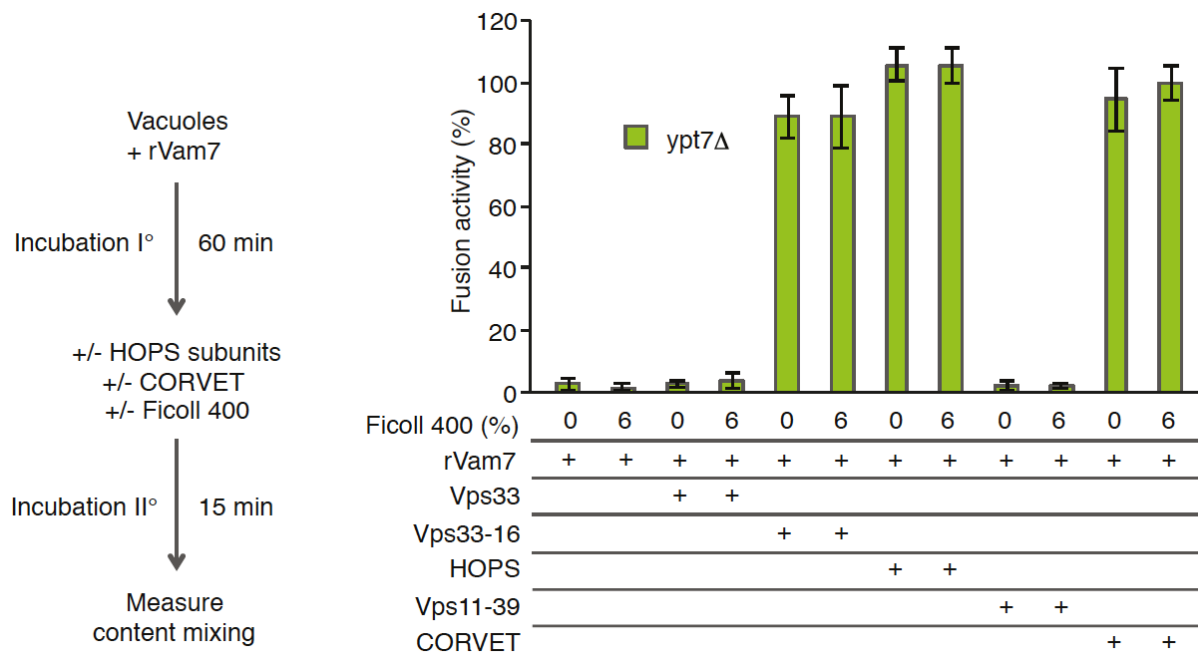


**Figure S3: HOPS and CORVET complexes stimulate fusion to similar degrees.**

Two-stage fusion reactions with *ypt7Δ* vacuoles were run as in Fig. 1g, in the absence of ATP. rVam7 had been added in the first phase of the incubation, 0.4μM HOPS subcomplexes or 0.4μM CORVET only in the second. Half of the samples received an addition of 6% of Ficoll 400 in the second incubation, an agent mimicking molecular crowding<sup>37</sup>. At the end of the 75 min incubation period, content mixing was assayed. Fusion activity of a standard wildtype reaction performed in the presence of ATP served as 100% reference. Means ± s.d. are shown. n=3.

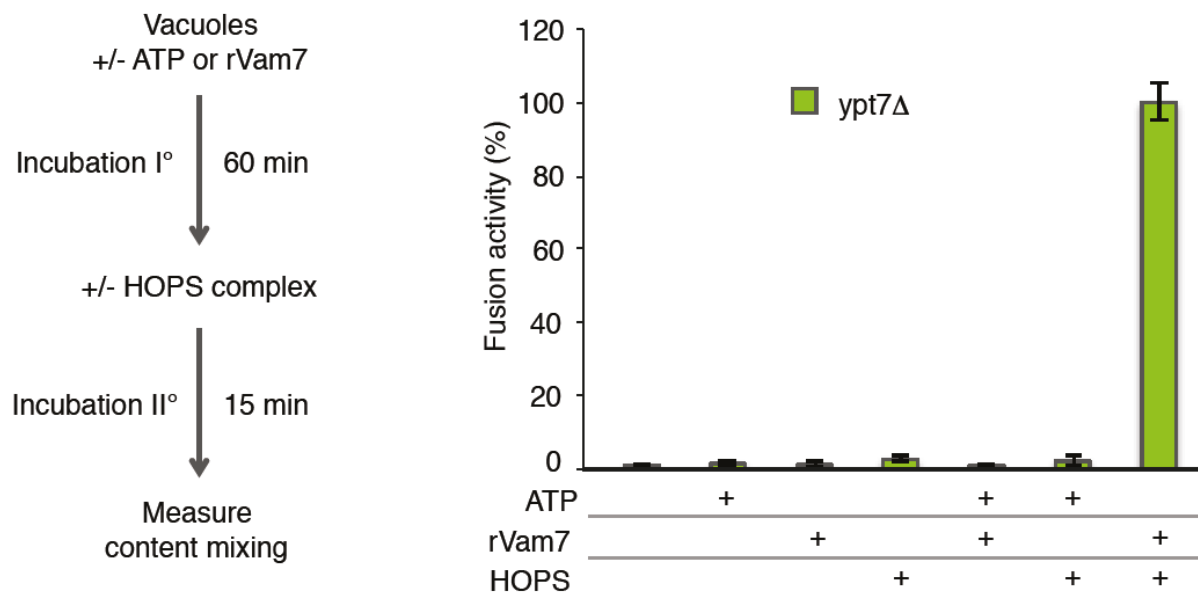


**Figure S4: *ypt7Δ* vacuoles require both Vam7 and HOPS for content mixing.**

Two-stage fusion reactions were run as in Fig. 1g in the presence or absence of ATP. rVam7 had been added in the first (I°) phase of the incubation, HOPS only in the second (II°). At the end of the 75 min incubation period, content mixing was assayed. Means  $\pm$  s.d. are shown. n=3.

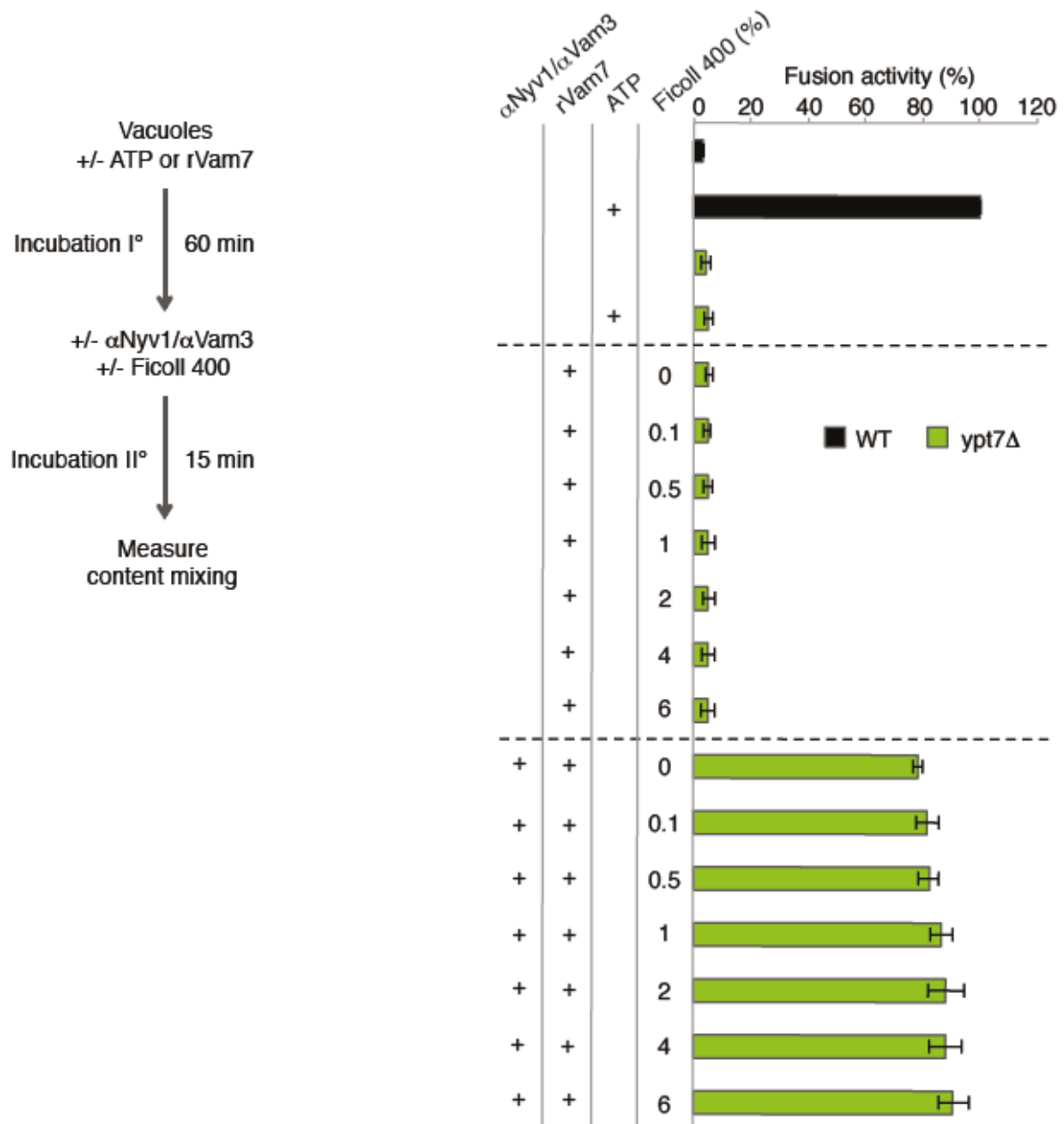


**Figure S5: A molecular crowding agent cannot stimulate fusion in the absence of bulky SNARE ligands.**

Two-stage fusion reactions with *ypt7 $\Delta$*  vacuoles were run as in Fig. 2b, in the absence or presence of ATP. rVam7 had been added in the first phase of the incubation where indicated, antibodies and various concentrations of the crowding agent Ficoll 400 only in the second. At the end of the 75 min incubation period, content mixing was assayed. Fusion activity of a wildtype reaction performed in the presence of ATP served as 100% reference. Means  $\pm$  s.d. are shown. n=3.

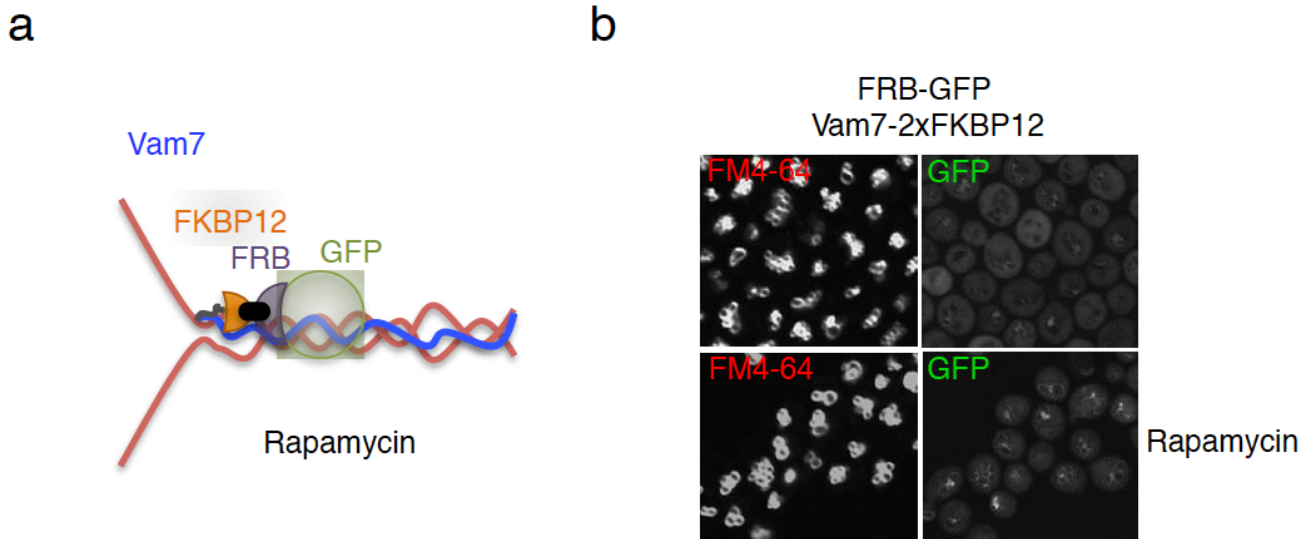


**Figure S6: Effect of rapamycin-induced dimerization on in-vivo vacuole fusion using the small fusion protein FRB-GFP.**

**a**, Schematic view of rapamycin-induced FKBP12/FRB-tagged protein dimerization between Vam7-2xFKBP12 and FRB-GFP. **b**, Logarithmically growing cells, expressing tagged Vam7-2xFKBP12, were stained with the vacuole tracer FM4-64 and analyzed by spinning disc microscopy before and 10 min after the addition of 10  $\mu$ M rapamycin. Scale bar: 5  $\mu$ m.

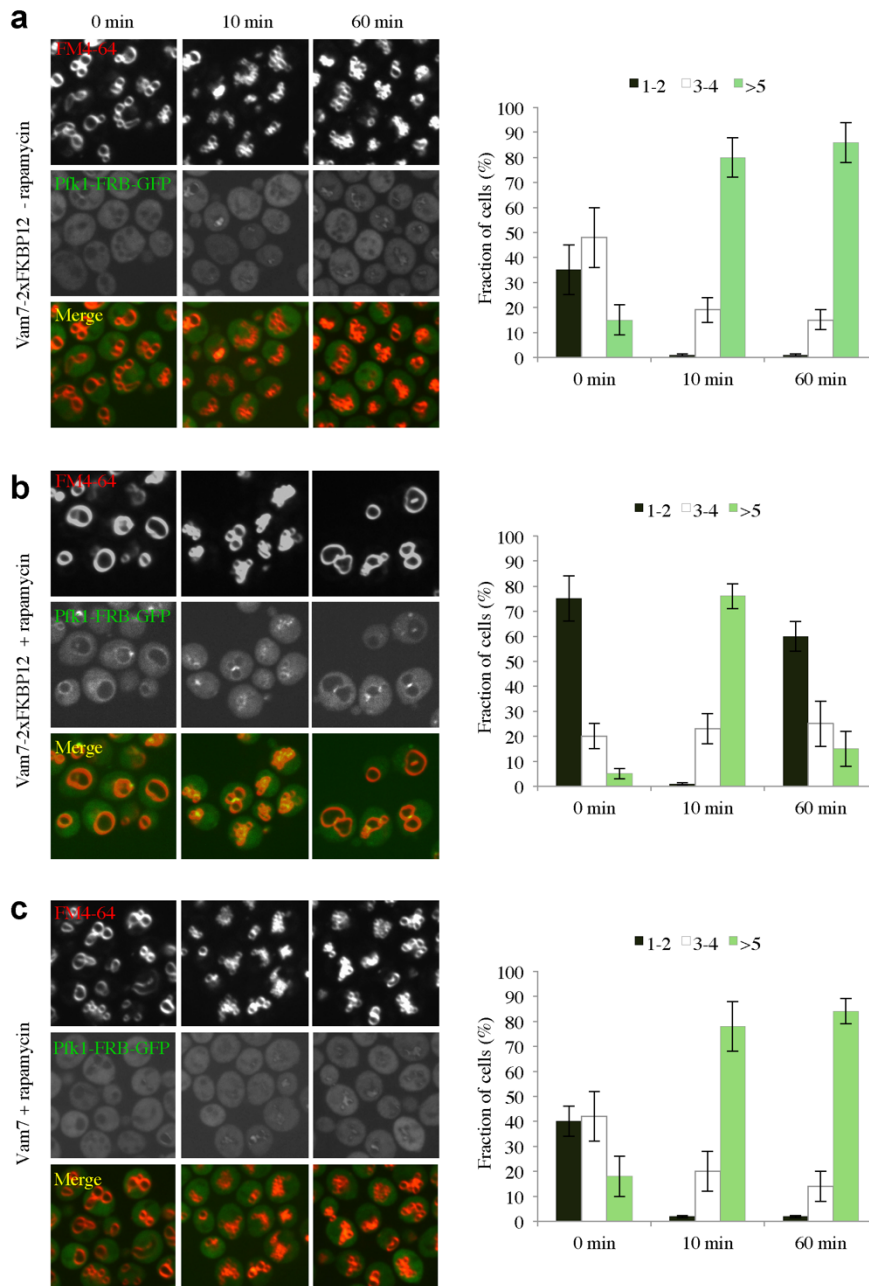


**Figure S7: Fusion can be prematurely triggered by protein recruitment after osmotically induced vacuole fragmentation.**

**a**, Logarithmically growing cells, carrying Vam7-2xFKBP12 and Pfk1-FRB-GFP as indicated, were stained with the vacuole tracer FM4-64. Vacuole fission was induced by adding 0.5 M NaCl. Cells were analyzed by spinning disc microscopy before and 10 and 60 min after salt addition. The cells were grouped into three categories according to the number of vacuoles visible per cell. 100 cells were analyzed per sample. Values represent the means and s.d.. n=3. Scale bar: 5  $\mu$ m. **b**, As in **a**, but 10  $\mu$ M rapamycin was added before the salt shock. **c**, As in **b**, but with cells expressing non-tagged Vam7.

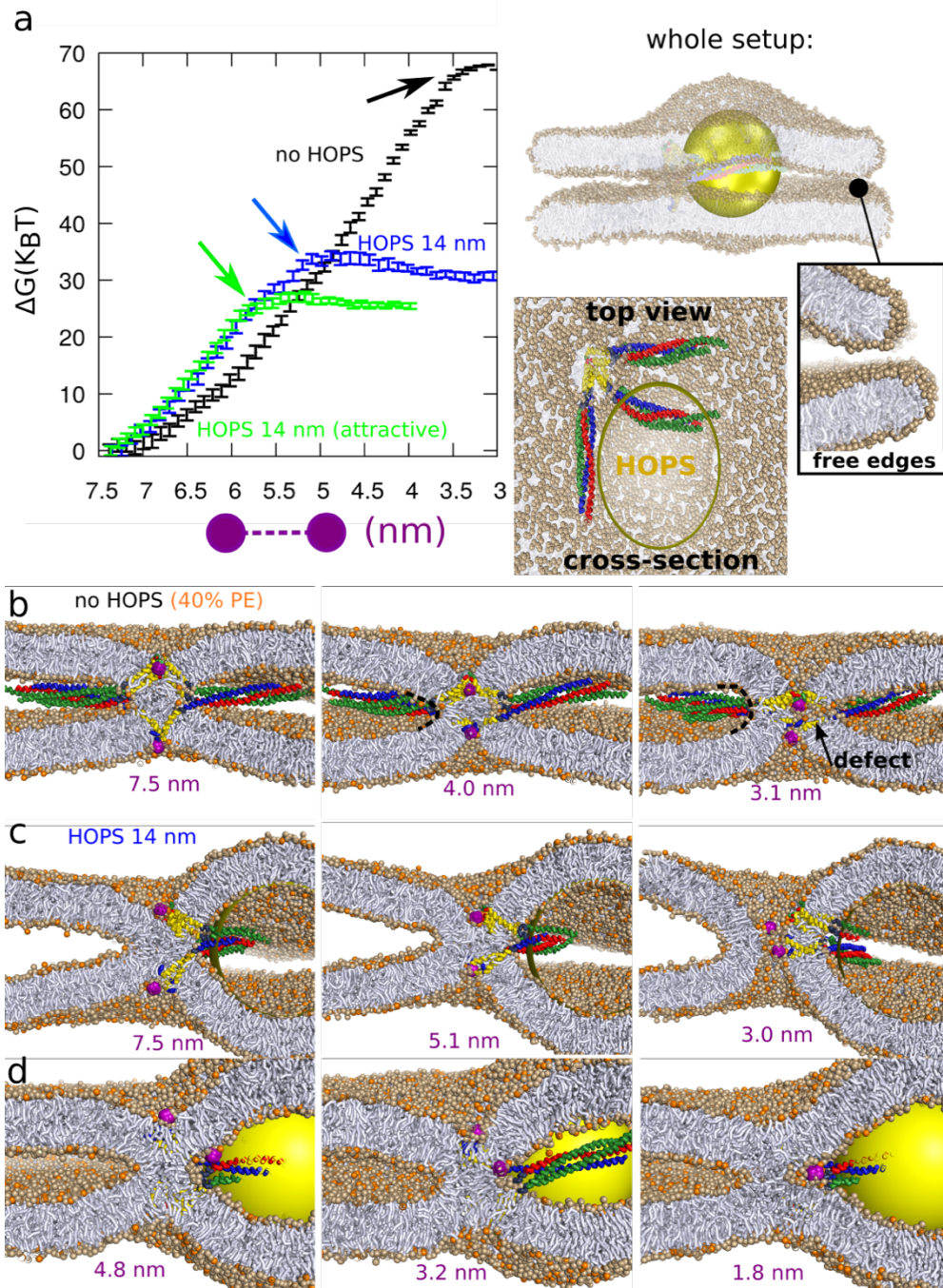


**Figure S8: Effect of HOPS on the free energy barrier of fusion pore formation.**

This plot complements Fig. 4 in the main manuscript.

**a.** The free energy barrier of fusion pore opening is derived for a simulated system consisting of 3 SNARE complexes (panels on the right side) and a POPC membrane that contains 40% POPE (colored orange). To this aim, we pull two hydrophilic probes (colored purple) towards the center of the stalk and estimate the work ( $\Delta G$ ) as a function of probe – probe distance (the stalk thickness)<sup>26</sup>. The arrows in the free energy profile (**a**) indicate the nucleation barrier for the fusion pore. Beyond this stage, subsequent pore opening proceeds in the absence of additional work (the

plateau region). Tethering proteins such as HOPS are attracted to the membrane through Rab-GTPases or direct lipid interaction<sup>21,22</sup>. An attractive 'HOPS' surface (green line) conserves the lowered nucleation barrier, even when the surface attractions fully compensate the membrane bending energy (no net bending work; Fig. S9). **b**, Pore formation in the absence of HOPS. A defect is frequently formed in the vicinity of the SNARE TMDs (black arrow), illustrating the presence of a high stress (the defect likely decreases the bending stress). Fusion pore formation is associated with a sudden reduction of the sharp curvature near the stalk's circumference (dashed lines). Fusion pores tend to adopt a teardrop shape<sup>28,29</sup>. **c**, Fusion pore formation in the presence of HOPS. The pre-existing teardrop membrane shape imposed by HOPS likely provides a geometrical and therefore an energetic advantage for pore formation. **d**, Setup where we artificially enforced formation of a leakage pore/defect in the direct vicinity of the stalk (the rationale behind this has been explained<sup>26</sup>). The induced defect (Between 3.2 and 1.8 nm the probe pierced through the membrane) instantaneously recovers. This suggests that the stress that HOPS imposes on the fusion site does not poise fusion to become leaky.

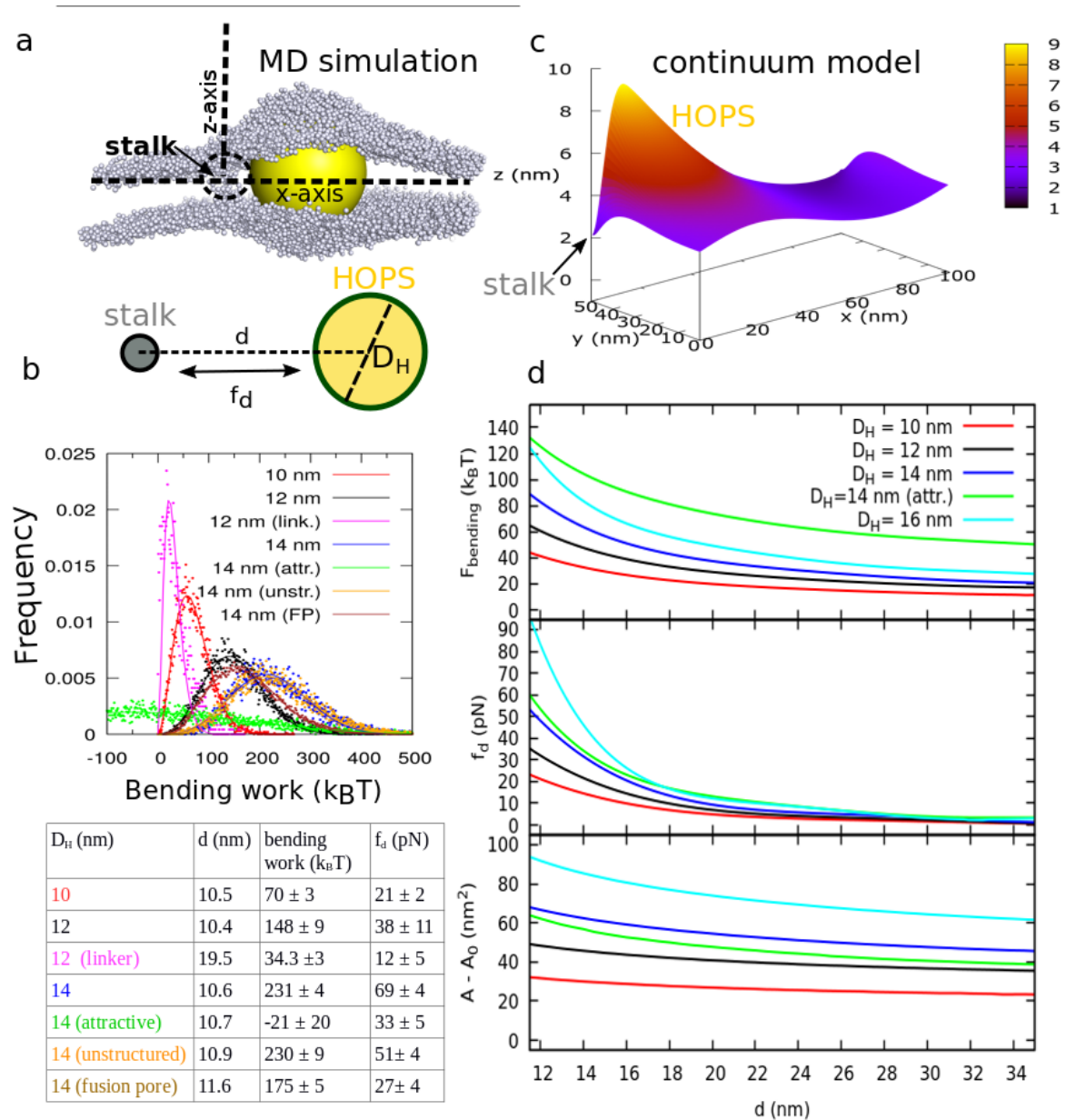


**Figure S9: Detailed analysis of HOPS-mediated membrane bending in the presence of an inter-membrane restraint.**

**a**, Simulation snapshot illustrating the geometry of the system. Shown is the central plane of the membrane (the lipid tail ends), the stalk, and HOPS. The SNARE complex present in the simulation setup is not illustrated. This setup serves as a motivation for the elastic continuum model.

**b**, Bending work required to place HOPS at the (hemi-)fusion site and peristaltic force experienced by HOPS. Simulations were run to measure the work required to place HOPS-like spheres of 10-14 nm diameter at the site of hemifusion or at a fusion pore (FP). HOPS could be detached from the SNARE complex by a long spacer (link.). The influence of a SNARE complex with an unstructured, non-helical

juxta-membrane region (unstr.) and of a HOPS mimic that was attractive to the membrane surface (attr.) was also analyzed. The lower panel shows averages obtained from the simulations.  $f_d$  is the (peristaltic) force that pushes HOPS away from the inter-membrane restraint (e.g., a stalk, fusion pore, or trans-SNARE complex). Note that surface attractions or Rab-GTPase interactions of HOPS (modeling the tethering of membranes)<sup>21,22</sup> can yield a negative value of the average work required to bend the membrane (bending occurs spontaneously). Fusion pore formation reduces the required bending work – it moves HOPS away from the restraint because of additional SNARE association up into the TMD region.

**c**, Elastic continuum model. The coordinate system is based on the snapshot of the molecular dynamics simulation shown in panel a. Because of symmetry along the xy-plane and xz-plane, we only model a quarter of the original system. The cartoon illustrates the shape of minimal free energy for a membrane (modeled by a single sheet), subjected to two constraints: (i) A local constraint on the position (height) of the membrane illustrated by the black arrow at  $z=2$  nm. This mimics the inter-membrane constraint (stalk, fusion pore or partly-assembled SNARE complex), (ii) The presence of a hemisphere. This mimics HOPS. The color code illustrates the height of the membrane (the z-axis) relative to the two constraints.

**d**, Prediction of bending energies by the elastic continuum model. The bending energy is shown as a function of the size and distance of HOPS to the inter-membrane restraint. Upper panel: Bending energy decreases steeply when HOPS moves away from the restraint. The predicted values are about a factor of two lower than the “bending work” predicted by the simulations (see *Methods*). Middle panel: the corresponding peristaltic force  $f_d$  on HOPS (the derivative of bending energy). At short distances,  $f_d$  becomes substantial (tens of pN). Note that making the surface of HOPS moderately attractive to the membrane affects  $f_d$  only weakly, i.e. it does not result in an attraction towards the 'stalk'. Lowest panel: The relative reduction of membrane area as a result of HOPS-induced membrane bending. This property reflects the tension that HOPS induces by curving the membrane near the contact zone. In contrast to bending energy and force, tension only weakly depends on the distance ( $d$ ) to the restraint.

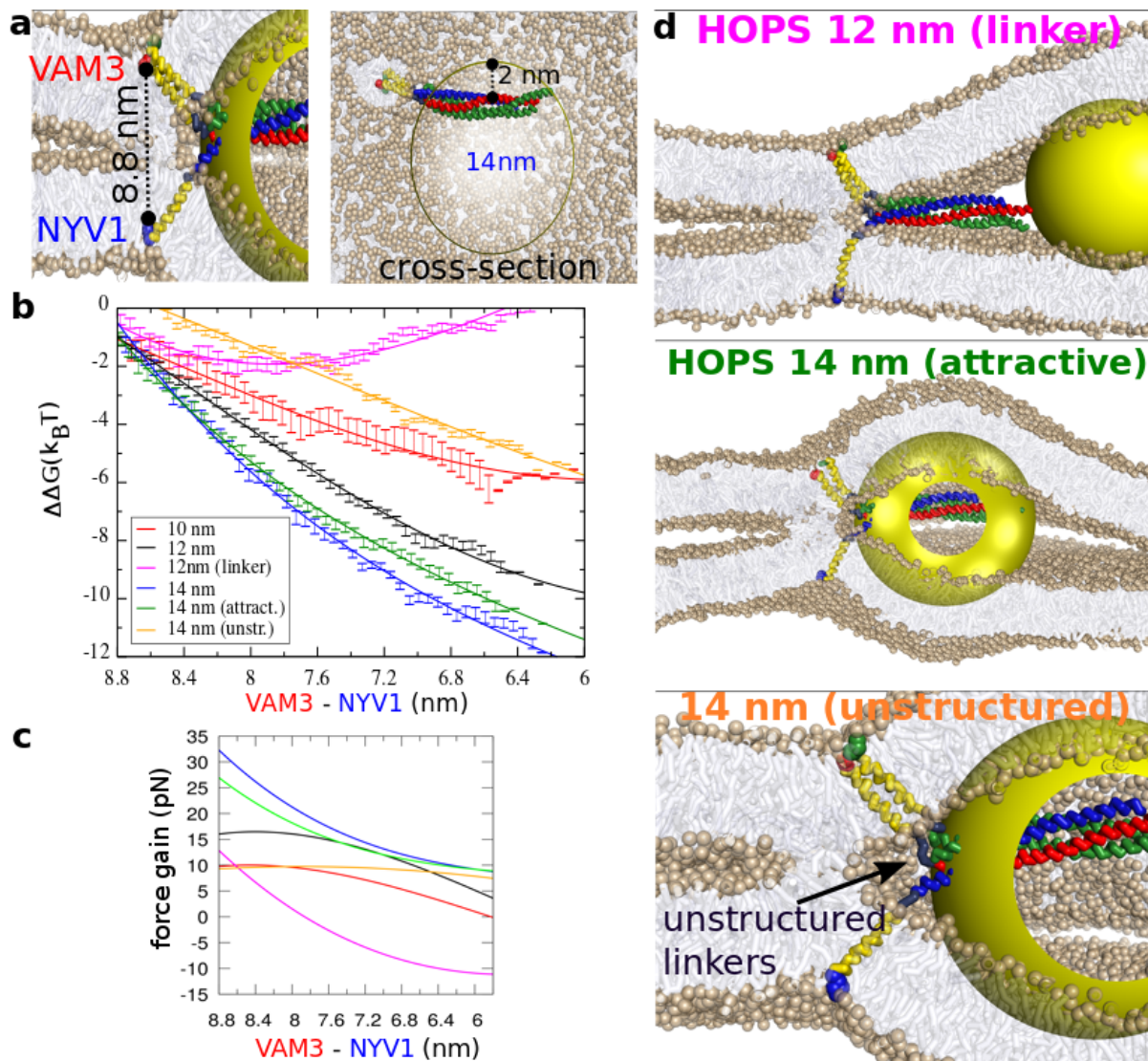


**Figure S10: Effect of HOPS on the force exerted by a single SNARE complex.**

**a**, One way of rationalizing the acceleration of fusion pore formation by a SNARE complex is to consider it as a mechanical device that exerts force on the luminal leaflets through its TMDs, thereby compressing the stalk. This can happen through a peristaltic force that pulls the SNARE complex away from the stalk, or through the elastic bending of the SNAREs. This latter mode of force transmission requires the juxta-membrane regions, which connect the coiled-coil domains of the SNAREs to their TMDs, to be structured and rigid. The compressing force that the SNARE complex exerts on the stalk can be rationalized from the apparent work (free energy) that one needs to perform in order to force the luminal C-termini of Vam3 and Nyv1 in closer proximity. We estimated how HOPS binding affects the force that the C-termini of the SNAREs Vam3 and Nyv1 exert on the stalk.

**b**, The work required to slightly indent the stalk in the presence of repulsive or

attractive HOPS-spheres of different diameter has been determined. It is shown relative to the situation without the sphere.

**c**, The corresponding forces on the SNARE TMDs were derived from this work. Apparent gains in the force exerted by the SNARE C-termini (left panel) are shown as a function of their distance in the hemifusion structure. HOPS binding can double or triple the magnitude of the apparent force (10-20 pN) that a SNARE complex exerts on a stalk <sup>47</sup>. The gain dissipates, however, as zipping of the SNARE TMDs progresses and their C-termini approach each other.

**d**, Snapshots of three special scenarios. Highest panel: The HOPS sphere is placed at a distal location with respect to the stalk (e.g., via attachment with a flexible linker). This abolishes the force gain. Middle panel: A sphere that favorably attracts (and bends) the membrane. This conserves the force gain. Lowest panel: Unstructured, flexible SNARE juxta-membrane regions partially disrupt the mechanical coupling between the coiled-coil domains and the TMDs. They decrease the apparent gain in SNARE pull force induced by HOPS. Structured ( $\alpha$ -helical) SNARE juxta-membrane regions result in a high initial force gain which gradually reduces. In contrast, unstructured, flexible juxta-membrane regions, which impair vacuole fusion <sup>48</sup> result in a near-constant force gain of only about 8 pN. Both cases converge to similar force values when the C-termini of Vam3 and Nyv1 come in closer proximity. Since the SNARE complex is unable to exert bending force on the membrane when the connection between its transmembrane anchors and the SNARE domains is completely flexible, we relate the remaining gain to an effective 'softening' of the stalk because of the induced membrane curvature and to the peristaltic force generated by the interaction of the HOPS sphere with the SNAREs.